Article

Cell Reports

Colony-Stimulating Factor 1 Receptor (CSF1R) Regulates Microglia Density and Distribution, but Not Microglia Differentiation *In Vivo*

Graphical Abstract

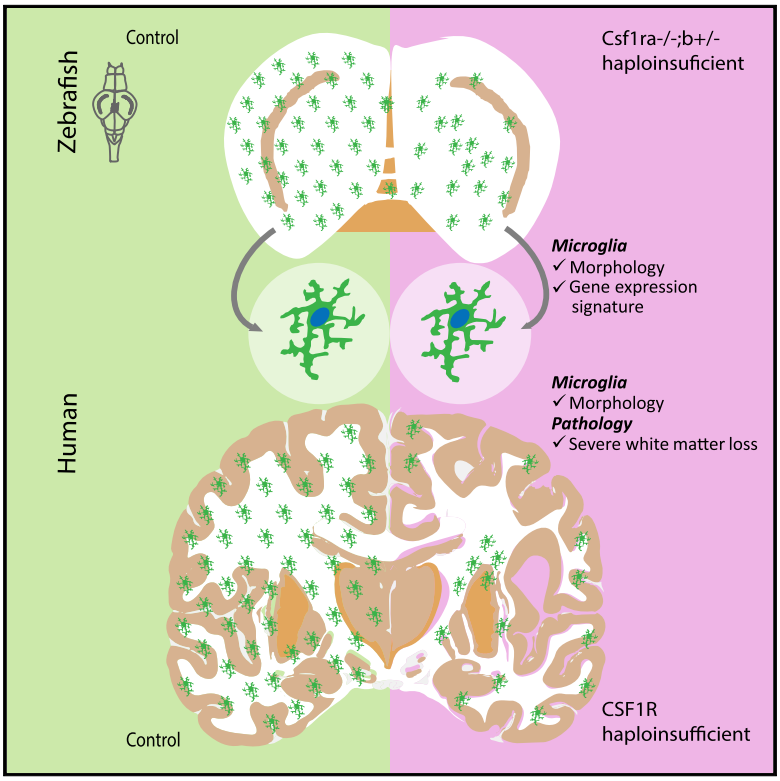

Highlights

- *csf1ra* and *csf1rb* together regulate microglia density in the adult zebrafish brain
- *csf1r* haploinsufficient microglia are normally differentiated and show normal signature
- *CSF1R* haploinsufficiency causes reduced microglia density and widespread depletion
- Microglia loss may be an early pathogenic event contributing to leukodystrophy

Authors

Nynke Oosterhof, Laura E. Kuil, Herma C. van der Linde, ..., Elly M. Hol, Mark H.G. Verheijen, Tjakko J. van Ham

Correspondence

t.vanham@erasmusmc.nl

In Brief

Oosterhof et al. show that colony-stimulating factor 1 receptor (CSF1R) primarily regulates microglia density and not their normal differentiation. In addition, they find widespread depletion of microglia in CSF1R-haploinsufficient zebrafish and leukodystrophy patients, also in the absence of pathology, indicating that microglia depletion may contribute to loss of white matter.

Oosterhof et al., 2018, Cell Reports *24*, 1203–1217
July 31, 2018
https://doi.org/10.1016/j.celrep.2018.06.113

CellPress

Cell Reports
Article

Colony-Stimulating Factor 1 Receptor (CSF1R) Regulates Microglia Density and Distribution, but Not Microglia Differentiation *In Vivo*

Nynke Oosterhof,[1] Laura E. Kuil,[1] Herma C. van der Linde,[1] Saskia M. Burm,[2] Woutje Berdowski,[1] Wilfred F.J. van Ijcken,[3] John C. van Swieten,[4,5] Elly M. Hol,[2,6] Mark H.G. Verheijen,[7] and Tjakko J. van Ham[1,8,*]

[1]Department of Clinical Genetics, Erasmus MC, University Medical Center Rotterdam, Wytemaweg 80, 3015 CN Rotterdam, the Netherlands
[2]Department of Translational Neuroscience, Brain Center Rudolf Magnus, University Medical Center Utrecht, Utrecht University, Utrecht, the Netherlands
[3]Center for Biomics, Erasmus MC, University Medical Center Rotterdam, Wytemaweg 80, 3015 CN Rotterdam, the Netherlands
[4]Department of Neurology, Erasmus MC, University Medical Center Rotterdam, Rotterdam, the Netherlands
[5]Department of Clinical Genetics, VU Medical Center, Amsterdam, the Netherlands
[6]Department of Neuroimmunology, Netherlands Institute for Neuroscience, an Institute of the Royal Netherlands Academy of Arts and Sciences, Amsterdam, the Netherlands
[7]Department of Molecular and Cellular Neurobiology, CNCR, Amsterdam Neuroscience, VU University, Amsterdam, the Netherlands
[8]Lead Contact
*Correspondence: t.vanham@erasmusmc.nl
https://doi.org/10.1016/j.celrep.2018.06.113

SUMMARY

Microglia are brain-resident macrophages with trophic and phagocytic functions. Dominant loss-of-function mutations in a key microglia regulator, colony-stimulating factor 1 receptor (CSF1R), cause adult-onset leukoencephalopathy with axonal spheroids and pigmented glia (ALSP), a progressive white matter disorder. Because it remains unclear precisely how *CSF1R* mutations affect microglia, we generated an allelic series of *csf1r* mutants in zebrafish to identify *csf1r*-dependent microglia changes. We found that *csf1r* mutations led to aberrant microglia density and distribution and regional loss of microglia. The remaining microglia still had a microglia-specific gene expression signature, indicating that they had differentiated normally. Strikingly, we also observed lower microglia numbers and widespread microglia depletion in postmortem brain tissue of ALSP patients. Both in zebrafish and in human disease, local microglia loss also presented in regions without obvious pathology. Together, this implies that CSF1R mainly regulates microglia density and that early loss of microglia may contribute to ALSP pathogenesis.

INTRODUCTION

Microglia are specialized brain macrophages whose functions in the brain include phagocytosis and provision of trophic support (Paolicelli et al., 2011; Safaiyan et al., 2016; Stevens et al., 2007; Tremblay et al., 2010; van Ham et al., 2012). Mutations in several genes that are highly expressed in microglia cause progressive white matter brain diseases (Meuwissen et al., 2016; Paloneva et al., 2002; Prinz and Priller, 2014; Rademakers et al., 2011). For example, dominant loss-of-function mutations in colony-stimulating factor 1 receptor (CSF1R) cause adult-onset leukoencephalopathy with axonal spheroids and pigmented glia (ALSP), also known as hereditary diffuse leukoencephalopathy with axonal spheroids (HDLS) (Konno et al., 2017; Wider et al., 2009). Even though low expression of *Csf1r* has been reported in some neurons in the hippocampus, the expression of *CSF1R* is almost exclusive to microglia, suggesting that ALSP pathogenesis involves microglia dysfunction (Luo et al., 2013). But where one study showed reduced microglia numbers in cortical layers 3 and 4 in postmortem end-stage ALSP brain sections, another showed increased microglia numbers during earlier ALSP disease stages (Oyanagi et al., 2017; Tada et al., 2016). The mechanism whereby heterozygous *CSF1R* mutations affect microglia and, consequently, brain homeostasis is still unknown. Insight into ALSP pathogenesis will therefore contribute to our understanding of microglia function in the vertebrate brain and of microglia involvement in other brain diseases.

Even though CSF1R signal transduction has been studied extensively in macrophages, it is not entirely clear how defective CSF1R signaling affects microglia *in vivo*. Activation by one of the two CSF1R ligands (CSF-1 or macrophage colony-stimulating factor [M-CSF]) or interleukin 34 (IL-34) leads to autophosphorylation of the tyrosine kinase receptor. *In vitro*, downstream activation of signal transduction pathways regulates the production, survival, differentiation, and function of macrophages (Dai et al., 2002; Erblich et al., 2011; Ginhoux et al., 2010; Wang et al., 2012). Genetic evidence for the consequences of CSF1R activation *in vivo* indicates that CSF1R primarily plays a homeostatic role in regulating the viability and proliferation of microglia (Cecchini et al., 1994; Jenkins et al., 2013). Indeed, genetic deficiency of CSF1R signaling reduces protection against bacterial infection, mainly by limiting macrophage supply (Cheers et al., 1989; Pagán et al., 2015; Teitelbaum et al., 1999; Wang et al., 2012). In contrast, by showing that

Csf1r$^{-/-}$ macrophage precursors have the same lineage potential as those in the wild-type, differentiating efficiently into macrophages but failing to form colonies, a recent study concluded that *Csf1r* deficiency has little effect on myeloid differentiation *in vivo* (Endele et al., 2017).

Loss of *Csf1r* in mice leads to an almost complete absence of microglia and also to severe developmental abnormalities and a shorter lifespan (Dai et al., 2002; Erblich et al., 2011; Ginhoux et al., 2010). *Csf1r*$^{-/-}$ brains show widened cerebral ventricles, which is also observed in ALSP patients. Mice lacking microglia also show cerebrovascular defects and reduced numbers of oligodendrocyte lineage cells (Erblich et al., 2011; Hagemeyer et al., 2017; Nandi et al., 2012). In addition, postnatal pharmacological inhibition of CSF1R in mice reduces the number of oligodendrocytes and oligodendrocyte precursor cells (OPCs) in a region-dependent manner (Hagemeyer et al., 2017). The latter effect could predispose to myelination defects later in life.

To understand the effect of CSF1R haploinsufficiency on microglia, we used the zebrafish as a model organism. Zebrafish are an upcoming genetic model organism to study brain diseases, including leukoencephalopathies (Zhang et al., 2016). They are highly suitable for *in vivo* imaging because they develop externally and are transparent at early stages (Haud et al., 2011; Oosterhof et al., 2015; Zhang et al., 2016). Previously, we identified the zebrafish microglia transcriptome, which shares high similarity with mouse and human microglia transcriptomes (Gosselin et al., 2017; Oosterhof et al., 2017). Zebrafish express two homologs of human *CSF1R*: *csf1ra* and *csf1rb*. We found that zebrafish *csf1ra* mutants show reduced microglia numbers only during development, partially mimicking mouse mutants. This suggests that the cellular functions of CSF1R are highly conserved between species but that zebrafish *csf1rb* and *csf1ra* are likely partially redundant. In the present study we therefore created an allelic series of zebrafish *csf1r* loss-of-function mutants in which we observed local loss of microglia, a general reduction in microglia numbers, and an aberrant distribution of microglia. Because we found that dysregulation of microglia density was a primary consequence of *csf1r* haploinsufficiency, we next investigated whether *CSF1R* haploinsufficiency also affects microglia density in postmortem brain tissue of ALSP patients. This revealed widespread depletion of microglia and a general reduction in microglia density. In humans and zebrafish alike, changes in microglia density and distribution in the absence of obvious myelin pathology implied that loss of microglia may be an early event in ALSP pathogenesis.

RESULTS

Zebrafish Csf1ra and Csf1rb Together Are Functionally Homologous to Mammalian CSF1R

To study how CSF1R mutations affect microglia and the brain, we exploited the fact that zebrafish have two homologs for human CSF1R: Csf1ra and Csf1rb. Both of these are highly expressed in adult zebrafish microglia (Figure 1A; Oosterhof et al., 2017). Unlike *Csf1r* knockout mice, which are almost completely devoid of microglia, zebrafish with homozygous loss-of-function mutations only in *csf1ra* (from here on called *csf1ra*$^{-/-}$), show reduced microglia numbers only during early development (Herbomel et al., 2001). This suggests that *csf1rb* and *csf1ra* share a role in microglia development.

To test this, we introduced a premature stop codon in exon 3 of the *csf1rb* gene by transcription activator-like effector nuclease (TALEN)-mediated genome editing and assessed microglia numbers by neutral red staining (Figures 1B and S1A), which can be used to label microglia in zebrafish larvae *in vivo*. Although the microglia numbers in homozygous *csf1rb* mutants were a little lower than in the wild-type, mutants deficient in both *csf1ra* and *csf1rb* (from here on called *csf1r*^{DM}), were almost completely devoid of microglia (Figures 1C and 1D). The absence of microglia in *csf1r*^{DM} mutants was confirmed in larval and adult zebrafish by immunostaining for L-plastin (Figures 1E, 2A, and 2B). Although microglia were almost completely absent in *csf1r*^{DM}, other macrophage populations were still present in adult organs, including the skin and the intestine (Figure S1B). Adult *csf1r*^{DM} animals were viable and, in-cross mating of *csf1r*^{DM} adult animals, produced viable homozygous mutant offspring (data not shown). However, after around 3 months of age, mutant animals occasionally showed seizure-like behavior, and their survival rate was lower than that of wild-type animals (data not shown). Some *csf1r*^{DM} brains displayed signs of cerebral hemorrhaging that were consistent with the hemorrhages previously reported in *Csf1r*$^{-/-}$ mice (Erblich et al., 2011). These data show that zebrafish Csf1ra and Csf1rb both regulate the development of the microglia population, and both are thus functionally homologous to mammalian CSF1R.

Csf1r Regulates Microglia Density and Distribution Independent of Brain Pathology

Previous studies indicate that the density of tissue macrophages, including microglia, is affected by reduced CSF1R signaling (Naito et al., 1991; Sasaki et al., 2000; Umeda et al., 1996; Wegiel et al., 1998). To validate this in zebrafish, we used neutral red labeling and immunohistochemistry to assess microglia numbers in a series of *csf1r* mutant zebrafish larvae consisting of *csf1ra*$^{+/-}$, *csf1ra*$^{-/-}$, *csf1rb*$^{-/-}$, *csf1ra*$^{-/-}$;*b*$^{+/-}$, and *csf1r*^{DM} animals. At the larval stage, a gradual reduction in the number of *csf1r* alleles resulted in a corresponding decrease in microglia numbers (Figures 1C–1E). The greater reduction in microglia numbers in *csf1ra*$^{-/-}$ mutants than in *csf1rb*$^{-/-}$ mutants suggests that *csf1ra* is more important during early development. In adult zebrafish, however, microglia numbers in *csf1rb*$^{-/-}$ mutants were strongly reduced, whereas, in *csf1ra*$^{-/-}$ mutants, they were more comparable with those in the wild-type (Figure 2C), suggesting differential requirements of *csf1ra* and *csf1rb* in microglia at different developmental stages. Surprisingly, in 5-month-old adult *csf1ra*$^{-/-}$;*b*$^{+/-}$ mutants, we observed that, although microglia were absent in the dorsolateral side of the optic tectum, they appeared to accumulate in the underlying deep brain regions (Figures 2A and 2B).

To investigate whether any pathological hallmarks of ALSP are also present in *csf1r* mutant zebrafish, we assessed tissue and white matter integrity in adult *csf1ra*$^{-/-}$, *csf1ra*$^{-/-}$;*b*$^{+/-}$, and *csf1r*^{DM} mutants. H&E labeling did not reveal signs of brain pathology (data not shown), nor did immunolabeling for Claudin K (Cldnk)—which labels myelin tracts throughout the zebrafish brain—reveal major loss of myelin, even in *csf1r*^{DM} mutants

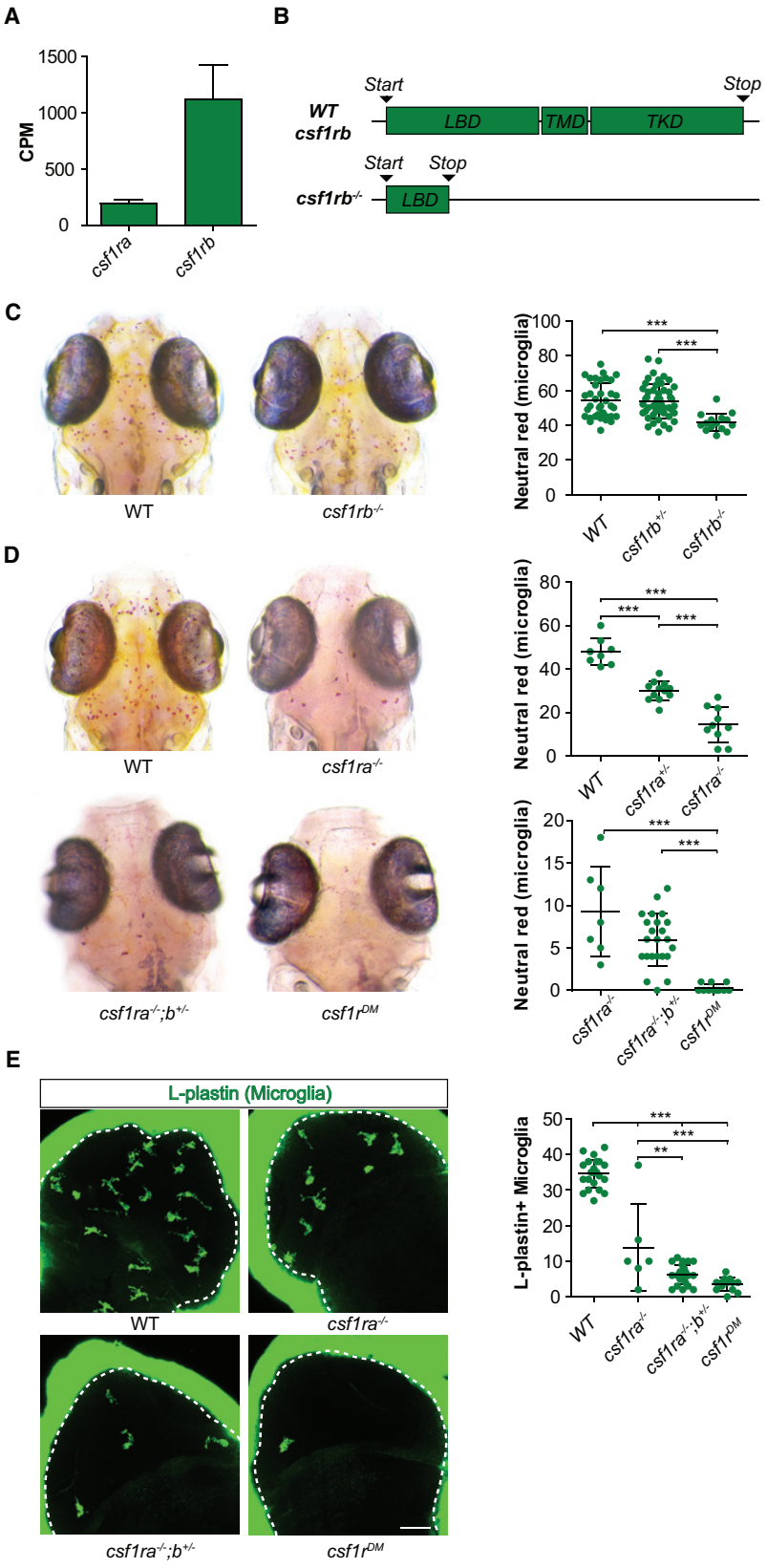

Figure 1. Microglia Numbers during Development Are *csf1r* Dosage-Dependent

(A) Counts per million (CPM) expression values of *csf1ra* and *csf1rb* from our previous RNA sequencing study in adult zebrafish microglia (Oosterhof et al., 2017).

(B) Schematic representation of the *csf1rb* mutation introduced with TALEN-mediated genome editing.

(C and D) 5 days post fertilization (dpf), WT, *csf1ra*$^{-/-}$, *csf1rb*$^{-/-}$, *csf1ra*$^{-/-}$;*b*$^{+/-}$, and *csf1r*^{DM} larvae were treated with neutral red for 2.5 hr. Images were acquired with a stereomicroscope, and microglia numbers were determined by counting the number of neutral red dots. n is at least 15 zebrafish/genotype for (C) and at least 7 for (D).

(E) 4 dpf, WT, *csf1ra*$^{-/-}$, *csf1ra*$^{-/-}$;*b*$^{+/-}$ and *csf1r*^{DM} were labeled with an antibody against L-plastin (Spangenberg et al., 2016), and L-plastin-positive cells were quantified in the optic tecti. n is at least 6 zebrafish/genotype.

LBD, ligand-binding domain; TMD, transmembrane domain; TKD, tyrosine kinase domain. Error bars represent SD. **p < 0.01, ***p < 0.001 (one-way ANOVA, Bonferroni multiple testing correction). Scale bar, 40 μm.

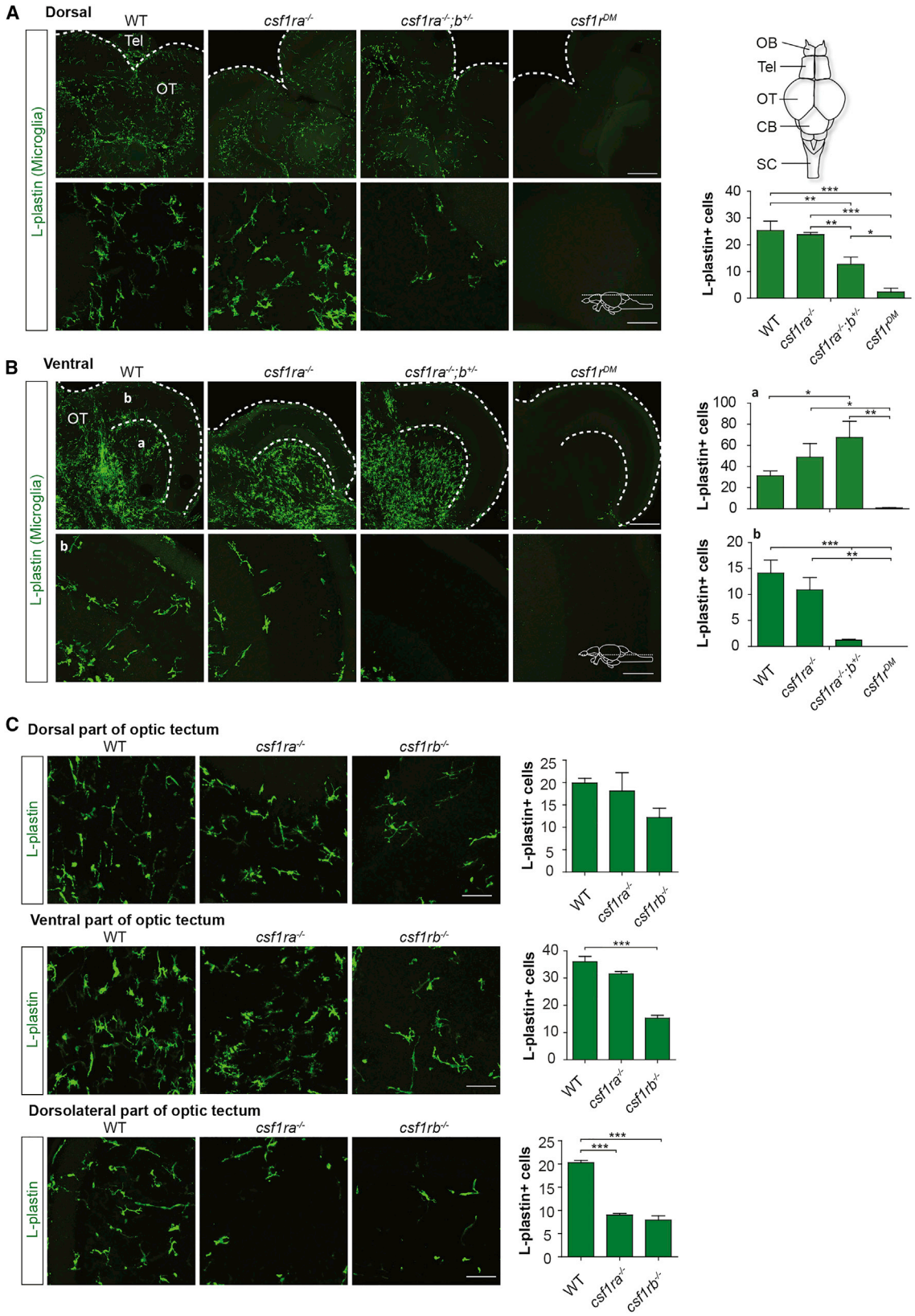

(legend on next page)

(Figure S2A; Münzel et al., 2012). To determine whether *csf1r* mutants display more subtle myelin abnormalities, such as degeneration, hypomyelination, or hypermyelination, we analyzed their white matter by electron microscopy (EM). We observed highly myelinated regions in the midbrain containing multilayered myelin sheets that resembled those in mammals but no apparent abnormalities in the multilayered myelin sheets in *csf1r* mutants (Figures S2B and S2C). Immunolabeling for Sox10 also indicated normal numbers of oligodendrocyte lineage cells in *csf1r* mutants (Figure S2D). Together, this indicates that *csf1r* deficiency in zebrafish does not result in overt myelin degeneration at this adult stage.

To establish whether loss of *csf1r* causes more subtle pathological changes, we performed RNA sequencing on brains of adult *csf1r* mutant zebrafish that were ~8 months old (Figure 3A). Multidimensional scaling of gene expression data showed clustering of the samples based on the *csf1r* mutation status (wild-type [WT], *csf1ra*$^{-/-}$, *csf1ra*$^{-/-}$;*b*$^{+/-}$, and *csf1r*^{DM}), indicating *csf1r*-dependent changes in gene expression (Figure 3B). Differential gene expression analysis between WT and *csf1r*^{DM} mutant brains revealed 154 differentially expressed genes, 85 of which (e.g., *spi1b*, *irf8*, *csf1ra*, and *csf1rb*) we had previously identified as part of the zebrafish microglial transcriptome (Figures 3C–3E; Table S2; Oosterhof et al., 2017). Hierarchical clustering of the samples on the basis of 154 differentially expressed genes revealed that *csf1ra*$^{-/-}$;*b*$^{+/-}$ mutants clustered with *csf1r*^{DM} mutants, whereas *csf1ra*$^{-/-}$ mutants clustered with the WT (Figure 3D). This suggests that loss of *csf1r* leads mainly to reduced expression of microglia-specific genes, which indicates that loss of *csf1r* in zebrafish predominantly affects microglia. The downregulated genes that were not specifically expressed in microglia included the cysteine-glutamine exchanger *slc7a11* and *growth hormone 1* as well as many poorly annotated genes (Table S2). This indicates that *csf1r* deficiency and, thus, loss of microglia causes very few molecular changes and no obvious myelin-related pathology in ~8-month-old adult zebrafish.

Csf1r-Deficient Microglia Increase the Expression of Genes Involved in Chemotaxis and Migration

To assess in more detail how *csf1r* deficiency affects microglia independently of brain pathology, we performed RNA sequencing on microglia that were sorted by fluorescence-activated cell sorting (FACS) from WT, *csf1ra*$^{-/-}$, and *csf1ra*$^{-/-}$;*b*$^{+/-}$ mutant brains that were dissected from ~9-month-old zebrafish (Figure 4A). Multidimensional scaling revealed clustering of the samples on the basis of *csf1r* mutation status, indicating *csf1r*-dependent changes in microglial gene expression (Figure 3B). Based on our microglia density measurements and the importance of *csf1rb* for adult microglia, we reasoned that *csf1ra*$^{-/-}$;*b*$^{+/-}$ mutant microglia could mimic the CSF1R haploinsufficiency that occurs in ALSP patient microglia and compared the microglia gene expression of these mutants with that of controls. We identified 1,466 genes that were differentially expressed between *csf1ra*$^{-/-}$;*b*$^{+/-}$ mutant and WT microglia (Figure 4C; Table S3). Interestingly, the normalized expression values of 750 of the 1,466 differentially expressed genes in *csf1ra*$^{-/-}$ mutant microglia lay in between those of *csf1ra*$^{-/-}$;*b*$^{+/-}$ and WT microglia (Figures 4C and 4D; Table S3). Because more than half of the genes differentially expressed between WT and *csf1ra*$^{-/-}$;*b*$^{+/-}$ show *csf1r*-dependent changes in expression, this indicates that these genes are regulated by Csf1r signaling, and their altered expression could be a primary consequence of *csf1r* deficiency. Gene ontology analysis of genes that showed *csf1r*-dependent changes in expression revealed that downregulated genes were associated with brain and nervous system development and with regulation of neuronal differentiation (Figure 4E). Upregulated genes were mainly associated with immune response, immune system process, and leukocyte chemotaxis (Figure 4F). The differentially expressed genes in the gene ontology classes associated with the upregulated genes were mainly chemokines and chemokine receptors (e.g., *cxcl12a*, *ccl25b*, *ccl19a.1*, and *cxcr4b*) (Figure 4G). In fact, the expression of most chemokines and chemokine receptors in zebrafish microglia was higher in *csf1ra*$^{-/-}$;*b*$^{+/-}$ mutants than in the WT (Figure 4G), which may explain the aberrant microglia distribution in *csf1ra*$^{-/-}$;*b*$^{+/-}$ mutants.

To test whether the expressional changes observed in *csf1ra*$^{-/-}$;*b*$^{+/-}$ microglia and the brain indicated a general microglia differentiation defect, we investigated whether adult *csf1r* mutants showed a loss of microglia-specific gene expression or a gain in gene expression associated with immature microglia or macrophages (Figures 4 and 5). Only 8 of the 300 most microglia-specific genes in zebrafish (many of which are also included in the mouse and human homeostatic microglia signature; e.g., *slco2b1*, *pdgfba*, and *scn4bb*) were significantly downregulated in *csf1ra*$^{-/-}$;*b*$^{+/-}$ microglia, suggesting that there is no loss of a homeostatic microglia signature (Figures 5A, 5D, and 5E; Butovsky et al., 2014; Gosselin et al., 2017; Oosterhof et al., 2017; Zhang et al., 2014).

Next we analyzed the expression of 378 zebrafish orthologs for genes that are strongly downregulated during microglia differentiation in the mouse brain to assess whether *csf1r* mutant microglia fail to downregulate genes specific to immature microglia (Matcovitch-Natan et al., 2016). Expression of only 10 of these 378 genes was increased in *csf1ra*$^{-/-}$;*b*$^{+/-}$ mutant microglia compared with the expression in WT microglia (Figures 5B and 5F). We also found no evidence for increased expression

Figure 2. Altered Microglia Distribution and Numbers in the Adult *csf1r* Mutant Brain

(A) Representative images of microglia in WT, *csf1ra*$^{-/-}$, *csf1ra*$^{-/-}$;*b*$^{+/-}$, and *csf1r*^{DM} brain sections from zebrafish aged 5 months post fertilization (mpf), stained with antibody against L-plastin (n = 3 zebrafish/group).

(B) Microglia in (a) the ventral part of the optic tectum and (b) the dorsolateral part of the optic tectum of WT, *csf1ra*$^{-/-}$, *csf1ra*$^{-/-}$;*b*$^{+/-}$, and *csf1r*^{DM}.

(C) Representative images of microglia in WT, *csf1ra*$^{-/-}$, and *csf1rb*$^{-/-}$ brain sections from 15 mpf zebrafish stained with antibody against L-plastin (n = 3 zebrafish/group).

Microglia were quantified in 3 areas (2.5 × 10^6 μm^3) per brain region per animal. Error bars represent SD. *p < 0.05, **p < 0.01, ***p < 0.001 (one-way ANOVA, Bonferroni multiple testing correction). Scale bars in (A) and (B), top, indicate 200 μm; in (A) and (B), bottom, and in (C), scale bars indicate 50 μm.

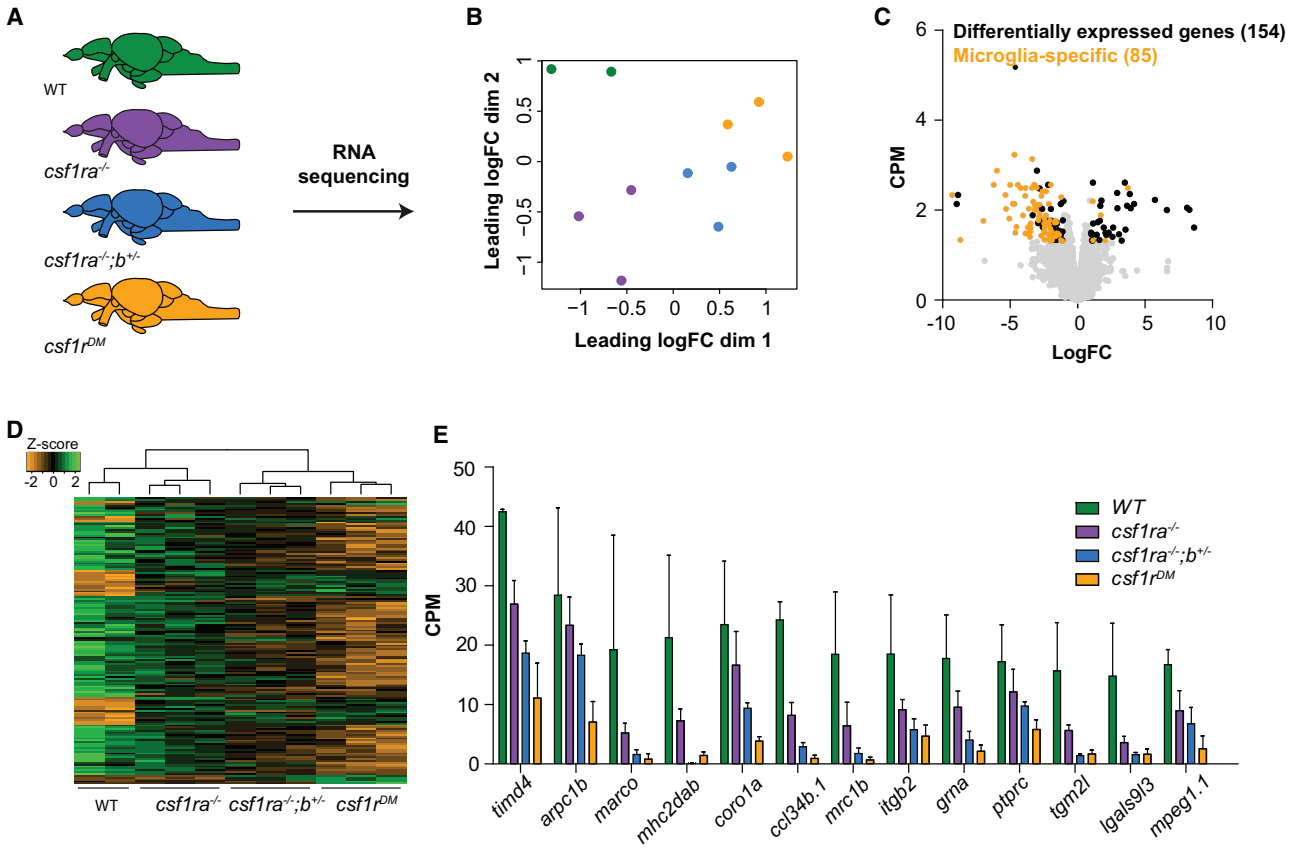

Figure 3. RNA Sequencing Reveals No Signs of Brain Pathology in *csf1r* Mutant Zebrafish

(A) Schematic representation of the whole-brain RNA sequencing experiment. RNA was isolated from whole brains of WT, *csf1ra*$^{-/-}$, *csf1ra*$^{-/-}$;*b*$^{+/-}$, and *csf1r*^{DM} fish (3 brains per sample, 2–3 samples per genotype).

(B) Multidimensional scaling plot.

(C) Volcano plot with genes differentially expressed between *csf1r*^{DM} and WT fish. Yellow dots represent genes that are part of the zebrafish microglia transcriptome (Oosterhof et al., 2017). Black dots represent the other differentially expressed genes. Gray dots represent all detected genes.

(D) Heatmap with genes differentially expressed between *csf1r*^{DM} and WT fish genes.

(E) Expression values of differentially expressed microglia-specific genes.

Genes were differentially expressed with false discovery rate (FDR) < 0.05 and log fold change (LogFC) > |1|.

of genes that discern microglia and macrophages (Figure 5C; Bennett et al., 2016). Additionally, *csf1ra*$^{-/-}$;*b*$^{+/-}$ microglia were still highly ramified and showed no signs of activation (Figure 5G). This suggests that the *csf1r*-dependent changes in microglial gene expression are largely independent of differentiation status. Together, these data imply that the changes in the expression of genes involved in chemotaxis and cell migration in *csf1r* mutants are a specific consequence of *csf1r* deficiency and not of a global differentiation defect.

The Damage-Induced Proliferative Response of *csf1r* Mutant Microglia Is Delayed

Microglia respond quickly to damage by migration and proliferation, and CSF1R has been linked to this proliferative response of microglia (Gómez-Nicola et al., 2013). Therefore, to assess whether proliferation defects could be linked to aberrant microglia localization and, possibly, to microglia migration, we used our previously established neuronal ablation model. In this model, metronidazole (MTZ) treatment in zebrafish with brain-specific transgenic expression of nitroreductase (NTR) results in neuronal cell death (van Ham et al., 2012, 2014). We have shown previously that increasing the local demand for microglia by inducing neuronal cell death causes a strong local proliferative response by microglia (Oosterhof et al., 2017). To investigate whether microglia proliferation depends on *csf1r* dosage, we used proliferating cell nuclear antigen (Pcna) as a cell proliferation marker to assess microglia proliferation upon induction of neuronal ablation. One day after treatment, control NTR transgenic larvae showed that the microglia numbers had increased from 25 to 32 locally, with a corresponding increase in the fraction of Pcna^{+} microglia (Figure 6A). In contrast, *csf1r* mutant microglia, upon MTZ treatment, showed a much larger increase in microglia numbers, respectively, from 5 to 24 and from 2 to ~12, but had not yet increased significantly in the fraction of Pcna^{+} microglia (Figure 6A). Therefore, the increased microglia numbers in treated *csf1r* mutants cannot be explained by the fraction of

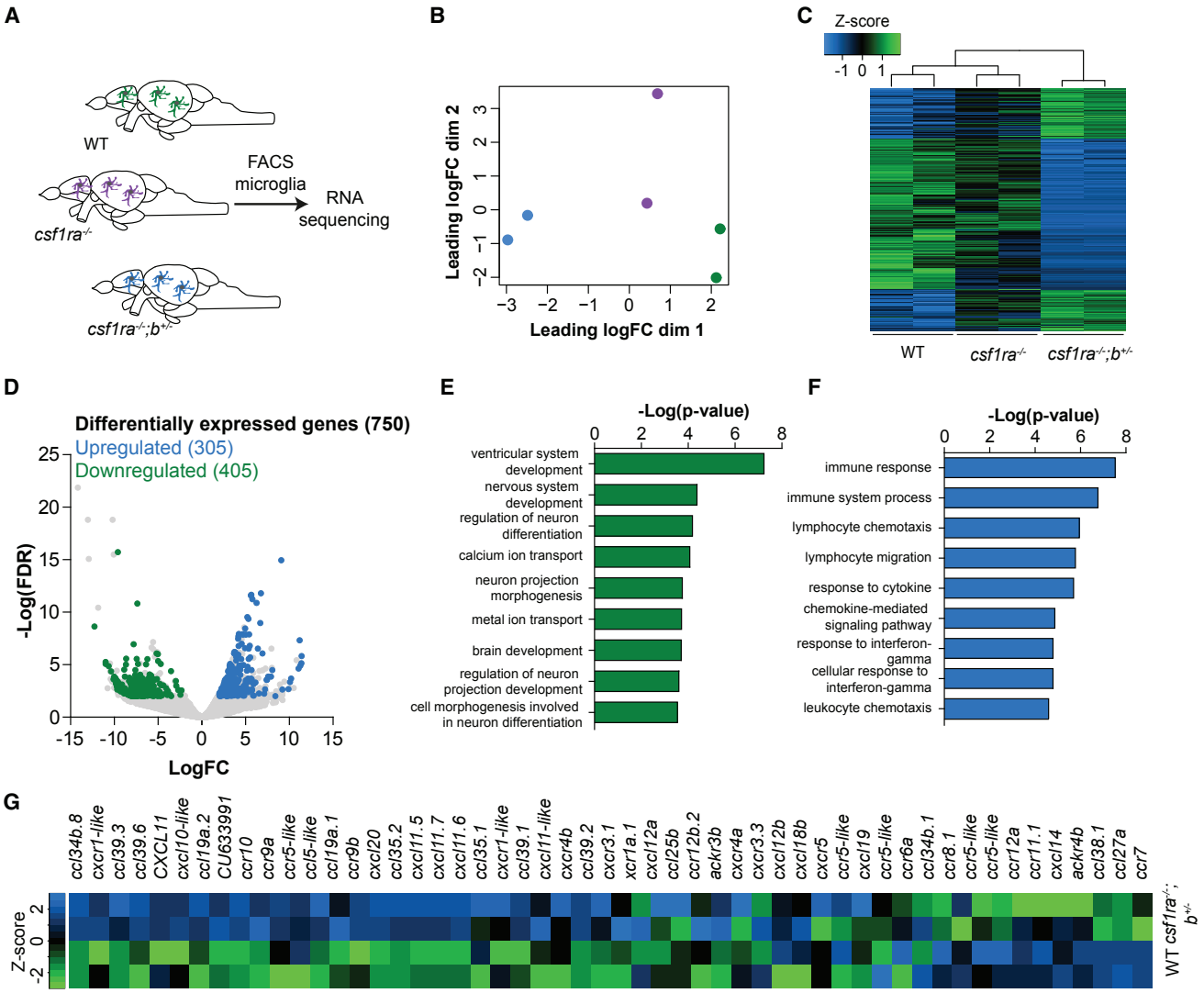

Figure 4. RNA Sequencing Reveals Increased Expression of Genes Associated with Chemotaxis in *csf1ra*$^{-/-}$;*b*$^{+/-}$ Mutant Microglia

(A) Schematic representation of the RNA sequencing experiment. Microglia were sorted by FACS from dissected brains from WT (3 brains per sample, 2 samples), *csf1ra*$^{-/-}$ (3 brains per sample, 2 samples), and *csf1ra*$^{-/-}$;*b*$^{+/-}$ (4–5 brains per sample, 2 samples) zebrafish.

(B) Multidimensional scaling plot.

(C) Heatmap of differentially expressed genes between *csf1ra*$^{-/-}$;*b*$^{+/-}$ and WT microglia.

(D) Volcano plot of differentially expressed genes (*csf1ra*$^{-/-}$;*b*$^{+/-}$ versus WT) whose expression values in *csf1ra*$^{-/-}$ mutants lay between those of WT and *csf1ra*$^{-/-}$;*b*$^{+/-}$ mutants.

(E and F) Gene ontology analysis was performed on genes that showed a *csf1r*-dependent decrease in expression (E) and increase in expression (F).

(G) Heatmap with expression *Z* scores for all chemokines and chemokine receptors that are expressed in zebrafish microglia.

Genes were differentially expressed with FDR < 0.01 and LogFC > |2|. Adult zebrafish used were between 9–12 months old.

dividing microglia relative to the control. Based on the much stronger increase in L-plastin+ cells in either of the mutants, however, one would expect a much higher fraction of Pcna^{+} cells in MTZ-treated cells versus controls if the increase is due to proliferation alone. Intriguingly, 2 days after treatment, the fractions of Pcna^{+} microglia were increased to similar levels in control and in *csf1r* mutants (Figure 6B). This showed that, although *csf1ra*$^{-/-}$ and *csf1ra*$^{-/-}$;*b*$^{+/-}$ mutant microglia were able to mount a proliferative response, the proliferative response was delayed. Nevertheless, because numbers still increased, it seems that potential initial proliferation deficiencies were compensated through microglia recruitment. Therefore, the aberrant distribution of microglia upon *csf1r* deficiency (Figures 2A and 2B) may be a compensatory mechanism intended to meet the brain's local demand for microglia.

Severe Microglia Depletion in Gray and White Matter of Postmortem ALSP Patient Brains

It has been reported that degenerated white matter in the brains of ALSP patients contains many CD68+ myeloid cells

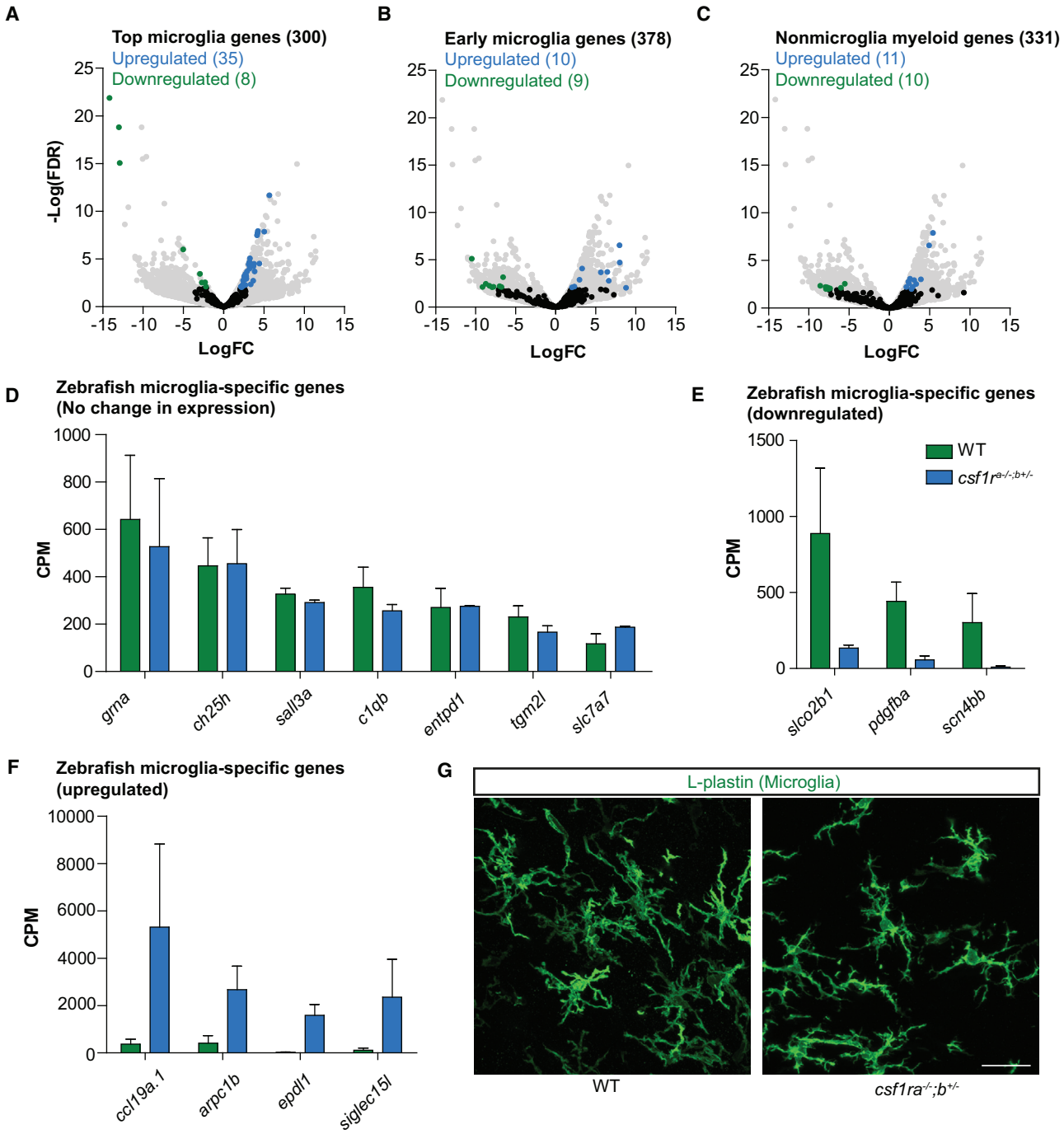

Figure 5. Differential Gene Expression of *csf1r*-Deficient Microglia Shows Normal Microglia Differentiation

(A) Volcano plot showing expressional changes of the 300 most highly expressed microglia-specific genes in *csf1ra*$^{-/-}$;*b*$^{+/-}$ mutant microglia (Oosterhof et al., 2017).

(B) Volcano plot showing the expressional changes in *csf1ra*$^{-/-}$;*b*$^{+/-}$ mutant microglia of normally downregulated genes during differentiation (Matcovitch-Natan et al., 2016) and of genes normally expressed in other macrophages in the CNS (Bennett et al., 2016).

(C) Volcano plot showing the expression changes of non-microglia myeloid genes.

(D) Expression values of zebrafish microglia-specific genes.

(E) Expression values of downregulated microglia-specific genes.

(F) Expression values of upregulated microglia-specific genes.

(G) Representative images of microglia (5-month-old fish) in the ventral part of the optic tectum labeled with an antibody against L-plastin. Scale bar, 20 μm.

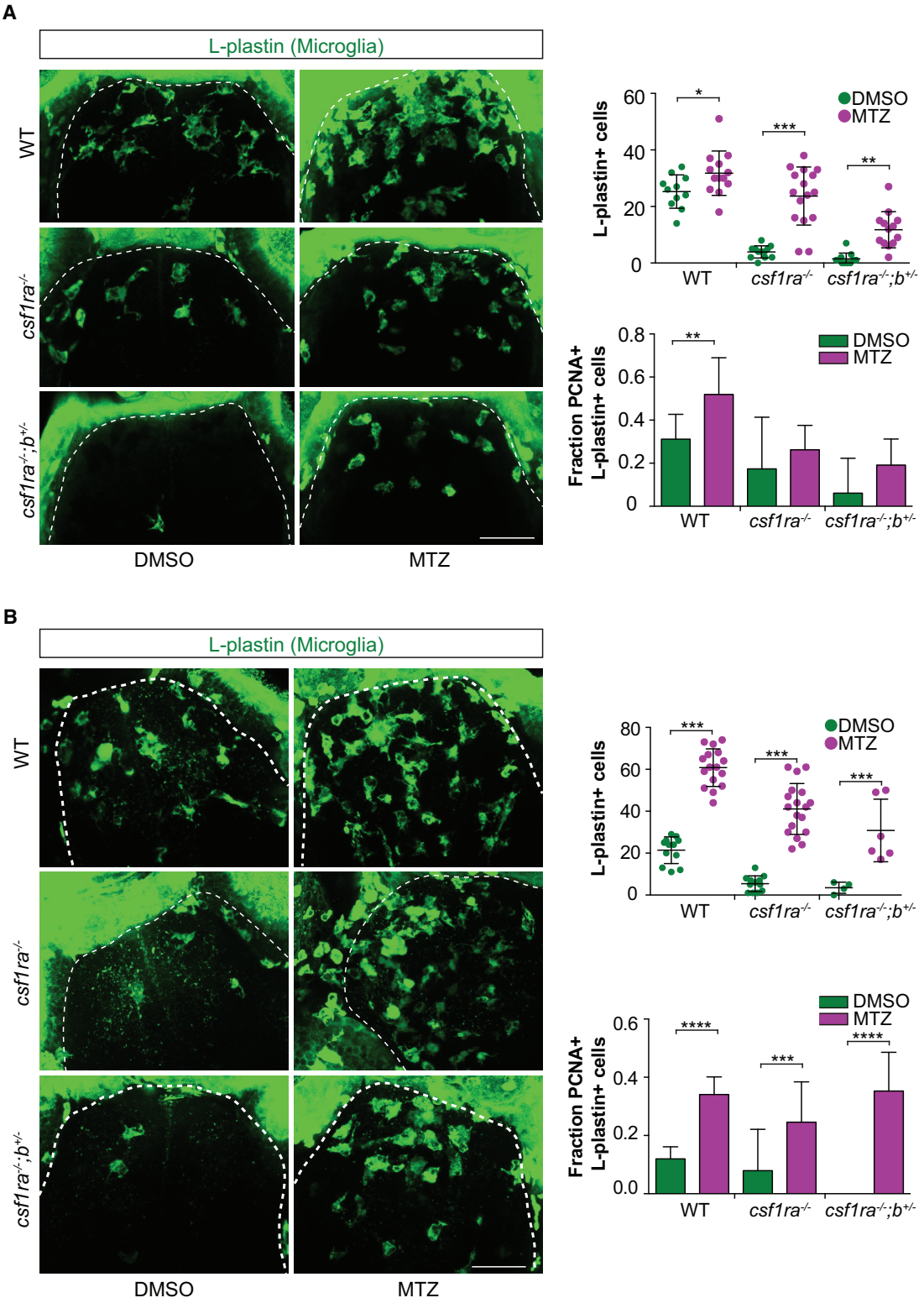

Figure 6. The Response to Neuronal Cell Death of *csf1r* Mutant Microglia Depends More on Recruitment Than on Proliferation

(A and B) We used our previously described conditional neuronal ablation model (van Ham et al., 2012, 2014), in which treatment with metronidazole (MTZ) leads to selective ablation of neurons with transgenic expression of NTR (the *nsfB* gene encoding NTR). WT, *csf1ra*$^{-/-}$, and *csf1ra*$^{-/-}$;*b*$^{+/-}$ larvae were

(legend continued on next page)

and reduced numbers of IBA1-positive microglia (Konno et al., 2014; Oyanagi et al., 2017; Tada et al., 2016). We wanted to investigate whether altered microglia density and distribution, as we identified in zebrafish, would recur in non-degenerated brain tissue of ALSP patients. By immunohistochemistry, we therefore analyzed microglia morphology, distribution, and density in gray matter, normal-appearing white matter (NAWM; occipital lobe), and degenerated white matter (middle frontal gyrus and cingulate gyrus) of two ALSP patients and age-matched controls (Figures 7 and S4A). As in previous studies, we observed numerous HLA-DR+ cells and large, rounded CD68+ cells in degenerated white matter, whereas, apart from a few IBA1/CD68-double-positive cells, IBA1+ cells were almost completely absent (Figures 7A, S3A–S3C, and S4B). Because we also observed a few CD68+ cells with a low level of IBA1 staining, this suggests that highly CD68+ cells lose IBA1 expression (Figure S3D).

Most IBA1+ microglia still present in the degenerated white matter appeared in clusters of ~10–100 cells (Figure 7B). Interestingly, with the exception of sparse microglia clusters, microglia in NAWM and gray matter were also severely depleted (Figures 7B, 7C, S3B, and S3C). Many of these IBA1+ microglia clusters were located at the border between the gray and the white matter (Figure 7B). Although the few IBA1+ cells present in the white matter looked like foam cells, microglia in the gray matter and NAWM either looked activated or had a normal ramified morphology (Figure 7B). In all brain areas examined, we also observed areas of gray matter in which IBA1+ microglia had a normal distribution and a ramified morphology. However, the density of these microglia was ~50% lower in ALSP patient brain sections than in controls (Figure 7D). This is reminiscent of the findings in our zebrafish experiments, where we also observed regional differences in microglia density in unaffected brain tissue (Figures 2 and 7B and 7D). The loss of IBA1+ microglia and the aberrant microglia distribution and altered morphology in microglia clusters—not only in the gray matter but also in NAWM—indicate that microglial changes could precede white matter degeneration.

Discussion

Although mutations in genes that are particularly important for microglia can cause severe brain disorders, it is still unclear whether pathogenesis involves a gain or loss of specific microglia activities. Here we used zebrafish to investigate the effect of a gradual reduction in functional *csf1r* alleles on microglia numbers and microglia differentiation status and their response to tissue damage. We found that Csf1r haploinsufficiency was correlated with a lower density of microglia in the dorsal part of the optic tectum. Additionally, we observed altered microglia distribution and local microglia depletion in the ventral and dorsolateral part of the optic tectum, respectively. Loss of three *csf1r* alleles did not severely impede the proliferative capacity of microglia to dying neurons, nor did it affect the homeostatic microglia signature. Instead, in response to increased phagocytic demand, *csf1r* mutant microglia initially increased their numbers locally through recruitment rather than proliferation. Accordingly, the expression of migration and chemotaxis genes in *csf1r* mutants was also increased. We also showed that, in the absence of extensive white matter degeneration in the occipital lobe of the cortex, CSF1R haploinsufficiency results in widespread depletion and aberrant distribution of IBA1+ microglia in humans. These findings support the presence of a disease mechanism in which CSF1R haploinsufficiency reduces microglia density, causes microglial relocation, and results in depletion of functional microglia.

Although the focus of this study is brain microglia, CSF1R haploinsufficiency could potentially affect other macrophages, such as those in the gut, or even neurons, because a low level of *Csf1r* expression was reported in a few scattered neurons in the mouse hippocampus (Luo et al., 2013). Because the composition of the gut microbiome or perturbed barrier function of the gut has major effects on microglia and on the CNS (Erny et al., 2015; Sampson et al., 2016) it is possible that, in ALSP patients, defects in other macrophage populations, such as those in the intestine, play a role in pathogenesis. Nevertheless, gastrointestinal symptoms related to perturbed gut barrier function were not reported in ALSP patients (Konno et al., 2017). Additionally, our zebrafish data do not imply an increased inflammatory response or response to microbial infection. Given that a potentially protective role of *Csf1r* has been described in neurons, it is possible that these protective effects are reduced due to *CSF1R* deficiency and could be a contributing factor in disease. Because neuronal loss is not obvious in ALSP patients, however, and severe phenotypes of $Csf1r^{-/-}$ mice are largely rescued by hematopoietic cells, we speculate that this is unlikely to play a major part (Bennett et al., 2018).

The CSF1R coding sequence and function are well conserved across species. CSF1R-deficient zebrafish, rodents, and, most likely, humans lack microglia, are osteopetrotic, and occasionally show cerebral hemorrhages (data not shown; Dai et al., 2002; Erblich et al., 2011; Ginhoux et al., 2010; Monies et al., 2017). Our data indicate that *csf1r* haploinsufficiency leads to local loss of microglia, possibly through maldistribution of microglia. This is similar to the aberrant distribution of microglia and widespread loss of microglia we observed in the NAWM and gray matter of postmortem ALSP patient brains. Interestingly, based on neuropathological analysis of different ALSP stages, in the early stages, microglia numbers were predicted to be higher than in controls, and microglia appear to be activated in specific brain regions (Oyanagi et al., 2017). This is reminiscent of the increased microglia density we observed in deep brain regions of $csf1ra^{-/-};b^{+/-}$ haploinsufficient zebrafish (Oyanagi et al., 2017). Similarly, microglia numbers are also higher in some brain regions in heterozygous *Csf1r* mutant mice than in

treated with MTZ at 5 dpf for 16 hr and fixed for immunohistochemistry (whole-mount) at 6 dpf (A) and 7 dpf (B). Immunostaining was performed for dividing ($Pcna^{+}$) microglia (L-plastin+), and the entire forebrain (dotted lines) was imaged and quantified. Scale bars, 40 μm. Group sizes were at least n = 10 zebrafish larvae (A) and at least n = 4 (B). Error bars indicate SD. *p < 0.05, **p < 0.01, ***p < 0.001, *p < 0.0001 (one-way ANOVA, Bonferroni multiple testing correction).

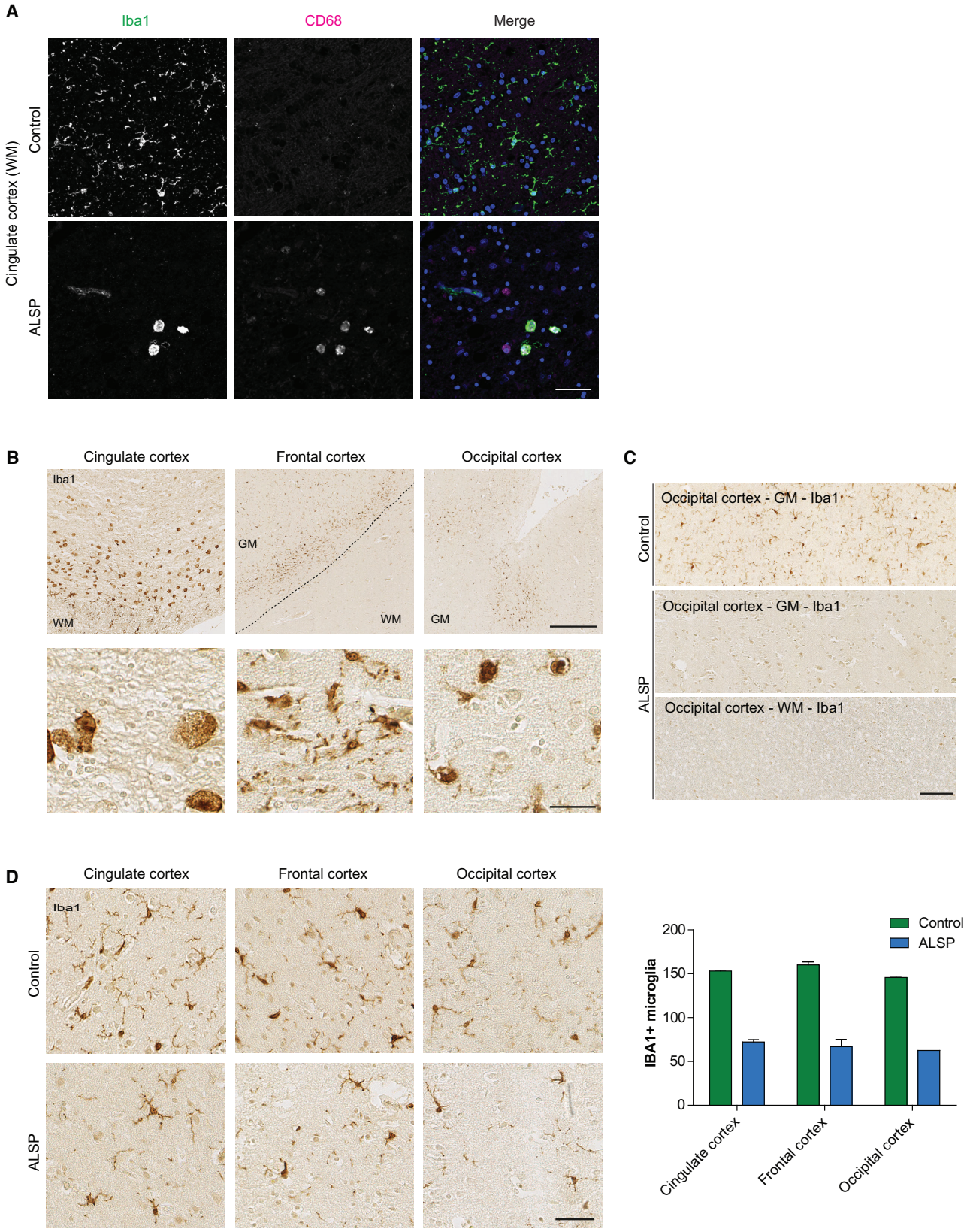

(legend on next page)

control animals, but it is unclear whether microglia density is reduced in other areas or at later stages in the mouse (Chitu et al., 2015). Between them, these observations indicate that *CSF1R* haploinsufficiency causes aberrant microglia distribution, where some regions become devoid of microglia.

Although microglia are efficient phagocytes that clear dead cells, dysfunctional synapses, and myelin (Ling, 1979; Safaiyan et al., 2016; Sierra et al., 2010), the accumulation of myelin debris in microglia can compromise their phagocytic capacity and can also lead to microglial senescence (Boven et al., 2006; Neumann et al., 2009; Safaiyan et al., 2016). Based on the size and morphology of large numbers of CD68+ cells in degenerated white matter, the accumulation of debris could have preceded their presence. We cannot exclude that CD68+ cells include infiltrated macrophages because other macrophage and microglia markers, including IBA1 and P2RY12, appear to be lost or very low in these cells (Tada et al., 2016). Regardless, accumulation of myelin debris, as occurs during normal aging, may contribute to the progressive loss of functional IBA1+ microglia over the course of the disease. In fact, it was shown in a tuberculosis infection model that, because of reduced *csf1r* signaling, the loss of macrophages was driven by a failure to meet phagocytic demand (Pagán et al., 2015). Consistent with this idea, the morphology of microglia among clusters in ALSP patients ranged from ramified to completely round and foamy in appearance, most likely because of the accumulation of phagocytized myelin debris in microglia (Boven et al., 2006). Simultaneously, it is possible that one functional *CSF1R* copy is not sufficient to sustain both normal microglia survival and proliferation because microglia turn over in humans in adulthood (Askew et al., 2017; Réu et al., 2017). Together, this indicates that CSF1R-dependent loss of microglia in ALSP patients may be progressive.

The absence of overt neuropathology or myelin pathology in *csf1r* mutant zebrafish may be related to their relatively young age, the fact that the CNS of the zebrafish is smaller and less complex than that of humans, or the time needed for the pathology to develop in humans. The pathological hallmarks of ALSP are observed mainly in the neocortex, which is unique to mammals and has expanded immensely during evolution, particularly in primates and humans (Florio and Huttner, 2014; Hofman, 2014). Because the neocortex is rich in white matter, it may be more susceptible to pathology than the zebrafish brain, in which there is relatively little white matter (Merrifield et al., 2017). Consistent with this, mutations that result in a relatively mild pathology in mice can lead to severe leukodystrophy in humans (Choquet et al., 2017). Additionally, it takes about 30–40 years before ALSP becomes symptomatic, whereas mice and zebrafish live only a few years (Konno et al., 2017). Even though the *csf1r* mutant zebrafish brain is relatively unaffected, the direct effects of *csf1r* mutations on microglia as described here were very similar to those in humans.

Although it is still unknown how long-term depletion of microglia in adulthood would affect brain homeostasis and how it might cause pathology, white matter degeneration is a hallmark of several other brain disorders classified as microgliopathies. For example, mutations in the microglia genes *TREM2* and *TYROBP* cause Nasu-Hakola disease (NHD), which is also characterized by white matter pathology. Even though the precise pathogenic mechanisms remain elusive, these disorders support the idea that microglia are critical to the maintenance of myelin in adulthood. In fact, it was recently shown in the adult brain that lower microglia numbers lead to a reduction in the numbers of oligodendrocytes or OPCs in many brain regions (Hagemeyer et al., 2017). We anticipate that a progressive depletion of microglia occurs in ALSP that could lead to a lower number of myelinating cells in adulthood and could contribute to ALSP pathogenesis.

Like tissue macrophages, microglia influence the development and repair of organs by secreting trophic factors, including insulin-like growth factor 1 (IGF1), and by mediating signaling between cells (Eom and Parichy, 2017; Wlodarczyk et al., 2017; Wynn et al., 2013). Local depletion of microglia could lead to a failure to provide such trophic factors, which could contribute to ALSP pathogenesis; for example, by affecting the capacity to form new oligodendrocytes.

In conclusion, the greatest effect of CSF1R haploinsufficiency seems to be a general reduction in microglia density in addition to large areas completely devoid of microglia. The partial or complete lack of microglia occurs in normal-appearing gray matter and NAWM, which suggests that loss of microglia may eventually result in ALSP pathology. Our gene expression data in an allelic series of *csf1r*-deficient microglia and brains therefore provide an opportunity to further delineate not only the function of *csf1r* in microglia but also the consequences for the brain. Elucidating these is crucial for a more comprehensive understanding of the physiological functions of microglia and microglia-dependent disease mechanisms. Several studies have shown that pharmacological inhibition of CSF1R causes microglia depletion and that, in mouse models, it ameliorates neurodegenerative disease-like symptoms by depleting microglia or diminishing their proliferation and activation (Elmore et al., 2014; Olmos-Alonso et al., 2016; Spangenberg et al., 2016). Because microglia depletion may underlie and contribute to

Figure 7. ALSP Patient Brains Show Widespread Microglia Depletion.

Shown are representative images of IBA1 and CD68 staining of microglia in white and gray matter of postmortem brain tissue of two ALSP patients and two age-matched control donors.

(A) IBA1 and CD68 double-labeling in the white matter of the cingulate gyrus of ALSP patient and control tissue.

(B) Clusters of IBA1+ microglia are apparent at the borders between the gray matter and the white matter.

(C) Severe depletion of IBA1+ microglia in the gray and white matter of the occipital cortex.

(D) The ramified morphology of microglia in gray matter areas of ALSP patients was similar to that in controls. Quantification of microglia numbers in gray matter areas of the cingulate cortex, frontal cortex, and occipital cortex showed a homogeneous distribution of ramified microglia (5 gray matter areas, 1.5 mm^2 in size, per brain region per patient). Error bars indicate SD.

Scale bars, 50 μm (A), 500 μm (B, low magnification), 30 μm (B, high magnification), 100 μm (C), 50 μm (D). WM, white matter; GM, gray matter.

the development and progression of ALSP, this raises the question of whether long-term inhibition of CSF1R in neurodegenerative diseases like Alzheimer's disease is a viable treatment option (Olmos-Alonso et al., 2016; Spangenberg et al., 2016). This warrants further studies to determine how the brain is affected by loss of microglia interactions and microglia-derived factors and to devise ways of promoting the supply of functional microglia.

STAR★METHODS

Detailed methods are provided in the online version of this paper and include the following:

- KEY RESOURCES TABLE
- CONTACT FOR REAGENT AND RESOURCE SHARING
- EXPERIMENTAL MODEL AND SUBJECT DETAILS
  - Animal models
- METHOD DETAILS
  - Vital dye labeling
  - Conditional neuronal cell death
  - Immunofluorescence staining
  - Luxol fast blue staining
  - RNA sequencing
  - Electron microscopy
- QUANTIFICATION AND STATISTICAL ANALYSIS
- DATA AND SOFTWARE AVAILABILITY

SUPPLEMENTAL INFORMATION

Supplemental Information includes four figures and three tables and can be found with this article online at https://doi.org/10.1016/j.celrep.2018.06.113.

ACKNOWLEDGMENTS

This work was sponsored by an Erasmus University Rotterdam fellowship, a ZonMW VENI grant (016.136.150), a Marie Curie Career Integration grant (322368), and an Alzheimer Nederland fellowship (WE.15-2012-01) (to T.J.v.H.) and an MKMD ZonMW grant (to E.M.H.). We thank Dr. B. Giepmans and A. Wolters (UMC Groningen) for advice regarding electron microscopy, T. van Gestel and Dr. G. Schaaf (Erasmus MC) for help with flow cytometry, the Netherlands Brain Bank for human brain tissue (coordinator Dr. I. Huitinga, Amsterdam, the Netherlands), and J. Wortel (VUMC) for her contribution to electron microscopy preparations.

AUTHOR CONTRIBUTIONS

Conceptualization, N.O. and T.J.v.H.; Methodology, N.O., H.C.v.d.L., and L.E.K.; Investigation, N.O., L.E.K., S.M.B., W.B., H.C.v.d.L., and M.H.G.V.; Formal Analysis, N.O.; Resources, W.F.J.v.I., E.M.H., and J.C.v.S.; Writing – Original Draft, N.O. and T.J.v.H.; Writing – Review & Editing, N.O., L.E.K., S.M.B., E.M.H., M.H.G.V., W.F.J.v.I., and T.J.v.H.; Supervision, T.J.v.H.; Funding Acquisition, T.J.v.H.

DECLARATION OF INTERESTS

The authors declare no competing interests.

Received: March 21, 2018
Revised: May 23, 2018
Accepted: June 27, 2018
Published: July 31, 2018

REFERENCES

Anders, S., Pyl, P.T., and Huber, W. (2015). HTSeq–a Python framework to work with high-throughput sequencing data. Bioinformatics *31*, 166–169.

Askew, K., Li, K., Olmos-Alonso, A., Garcia-Moreno, F., Liang, Y., Richardson, P., Tipton, T., Chapman, M.A., Riecken, K., Beccari, S., et al. (2017). Coupled Proliferation and Apoptosis Maintain the Rapid Turnover of Microglia in the Adult Brain. Cell Rep. *18*, 391–405.

Bennett, M.L., Bennett, F.C., Liddelow, S.A., Ajami, B., Zamanian, J.L., Fernhoff, N.B., Mulinyawe, S.B., Bohlen, C.J., Adil, A., Tucker, A., et al. (2016). New tools for studying microglia in the mouse and human CNS. Proc. Natl. Acad. Sci. USA *113*, E1738–E1746.

Bennett, F.C., Bennett, M.L., Yaqoob, F., Mulinyawe, S.B., Grant, G.A., Hayden Gephart, M., Plowey, E.D., and Barres, B.A. (2018). A Combination of Ontogeny and CNS Environment Establishes Microglial Identity. Neuron *98*, 1170–1183.e8.

Boven, L.A., Van Meurs, M., Van Zwam, M., Wierenga-Wolf, A., Hintzen, R.Q., Boot, R.G., Aerts, J.M., Amor, S., Nieuwenhuis, E.E., and Laman, J.D. (2006). Myelin-laden macrophages are anti-inflammatory, consistent with foam cells in multiple sclerosis. Brain *129*, 517–526.

Butovsky, O., Jedrychowski, M.P., Moore, C.S., Cialic, R., Lanser, A.J., Gabriely, G., Koeglsperger, T., Dake, B., Wu, P.M., Doykan, C.E., et al. (2014). Identification of a unique TGF-β-dependent molecular and functional signature in microglia. Nat. Neurosci. *17*, 131–143.

Camargo, N., Goudriaan, A., van Deijk, A.F., Otte, W.M., Brouwers, J.F., Lodder, H., Gutmann, D.H., Nave, K.A., Dijkhuizen, R.M., Mansvelder, H.D., et al. (2017). Oligodendroglial myelination requires astrocyte-derived lipids. PLoS Biol. *15*, e1002605.

Cecchini, M.G., Dominguez, M.G., Mocci, S., Wetterwald, A., Felix, R., Fleisch, H., Chisholm, O., Hofstetter, W., Pollard, J.W., and Stanley, E.R. (1994). Role of colony stimulating factor-1 in the establishment and regulation of tissue macrophages during postnatal development of the mouse. Development *120*, 1357–1372.

Cermak, T., Doyle, E.L., Christian, M., Wang, L., Zhang, Y., Schmidt, C., Baller, J.A., Somia, N.V., Bogdanove, A.J., and Voytas, D.F. (2011). Efficient design and assembly of custom TALEN and other TAL effector-based constructs for DNA targeting. Nucleic Acids Res. *39*, e82.

Cheers, C., Hill, M., Haigh, A.M., and Stanley, E.R. (1989). Stimulation of macrophage phagocytic but not bactericidal activity by colony-stimulating factor 1. Infect. Immun. *57*, 1512–1516.

Chitu, V., Gokhan, S., Gulinello, M., Branch, C.A., Patil, M., Basu, R., Stoddart, C., Mehler, M.F., and Stanley, E.R. (2015). Phenotypic characterization of a Csf1r haploinsufficient mouse model of adult-onset leukodystrophy with axonal spheroids and pigmented glia (ALSP). Neurobiol. Dis. *74*, 219–228.

Choquet, K., Yang, S., Moir, R.D., Forget, D., Larivière, R., Bouchard, A., Poitras, C., Sgarioto, N., Dicaire, M.J., Noohi, F., et al. (2017). Absence of neurological abnormalities in mice homozygous for the Polr3a G672E hypomyelinating leukodystrophy mutation. Mol. Brain *10*, 13.

Dai, X.M., Ryan, G.R., Hapel, A.J., Dominguez, M.G., Russell, R.G., Kapp, S., Sylvestre, V., and Stanley, E.R. (2002). Targeted disruption of the mouse colony-stimulating factor 1 receptor gene results in osteopetrosis, mononuclear phagocyte deficiency, increased primitive progenitor cell frequencies, and reproductive defects. Blood *99*, 111–120.

Davison, J.M., Akitake, C.M., Goll, M.G., Rhee, J.M., Gosse, N., Baier, H., Halpern, M.E., Leach, S.D., and Parsons, M.J. (2007). Transactivation from Gal4-VP16 transgenic insertions for tissue-specific cell labeling and ablation in zebrafish. Dev. Biol. *304*, 811–824.

Durinck, S., Spellman, P.T., Birney, E., and Huber, W. (2009). Mapping identifiers for the integration of genomic datasets with the R/Bioconductor package biomaRt. Nat. Protoc. *4*, 1184–1191.

Ellett, F., Pase, L., Hayman, J.W., Andrianopoulos, A., and Lieschke, G.J. (2011). mpeg1 promoter transgenes direct macrophage-lineage expression in zebrafish. Blood *117*, e49–e56.

Elmore, M.R., Najafi, A.R., Koike, M.A., Dagher, N.N., Spangenberg, E.E., Rice, R.A., Kitazawa, M., Matusow, B., Nguyen, H., West, B.L., and Green, K.N. (2014). Colony-stimulating factor 1 receptor signaling is necessary for microglia viability, unmasking a microglia progenitor cell in the adult brain. Neuron *82*, 380–397.

Endele, M., Loeffler, D., Kokkaliaris, K.D., Hilsenbeck, O., Skylaki, S., Hoppe, P.S., Schambach, A., Stanley, E.R., and Schroeder, T. (2017). CSF-1-induced Src signaling can instruct monocytic lineage choice. Blood *129*, 1691–1701.

Eom, D.S., and Parichy, D.M. (2017). A macrophage relay for long-distance signaling during postembryonic tissue remodeling. Science *355*, 1317–1320.

Erblich, B., Zhu, L., Etgen, A.M., Dobrenis, K., and Pollard, J.W. (2011). Absence of colony stimulation factor-1 receptor results in loss of microglia, disrupted brain development and olfactory deficits. PLoS ONE *6*, e26317.

Erny, D., Hrabě de Angelis, A.L., Jaitin, D., Wieghofer, P., Staszewski, O., David, E., Keren-Shaul, H., Mahlakoiv, T., Jakobshagen, K., Buch, T., et al. (2015). Host microbiota constantly control maturation and function of microglia in the CNS. Nat. Neurosci. *18*, 965–977.

Florio, M., and Huttner, W.B. (2014). Neural progenitors, neurogenesis and the evolution of the neocortex. Development *141*, 2182–2194.

Ginhoux, F., Greter, M., Leboeuf, M., Nandi, S., See, P., Gokhan, S., Mehler, M.F., Conway, S.J., Ng, L.G., Stanley, E.R., et al. (2010). Fate mapping analysis reveals that adult microglia derive from primitive macrophages. Science *330*, 841–845.

Gómez-Nicola, D., Fransen, N.L., Suzzi, S., and Perry, V.H. (2013). Regulation of microglial proliferation during chronic neurodegeneration. J. Neurosci. *33*, 2481–2493.

Gosselin, D., Skola, D., Coufal, N.G., Holtman, I.R., Schlachetzki, J.C.M., Sajti, E., Jaeger, B.N., O'Connor, C., Fitzpatrick, C., Pasillas, M.P., et al. (2017). An environment-dependent transcriptional network specifies human microglia identity. Science *356*, eaal3222.

Hagemeyer, N., Hanft, K.M., Akriditou, M.A., Unger, N., Park, E.S., Stanley, E.R., Staszewski, O., Dimou, L., and Prinz, M. (2017). Microglia contribute to normal myelinogenesis and to oligodendrocyte progenitor maintenance during adulthood. Acta Neuropathol. *134*, 441–458.

Haud, N., Kara, F., Diekmann, S., Henneke, M., Willer, J.R., Hillwig, M.S., Gregg, R.G., Macintosh, G.C., Gärtner, J., Alia, A., and Hurlstone, A.F. (2011). rnaset2 mutant zebrafish model familial cystic leukoencephalopathy and reveal a role for RNase T2 in degrading ribosomal RNA. Proc. Natl. Acad. Sci. USA *108*, 1099–1103.

Herbomel, P., Thisse, B., and Thisse, C. (2001). Zebrafish early macrophages colonize cephalic mesenchyme and developing brain, retina, and epidermis through a M-CSF receptor-dependent invasive process. Dev. Biol. *238*, 274–288.

Hofman, M.A. (2014). Evolution of the human brain: when bigger is better. Front. Neuroanat. *8*, 15.

Hovens, I.B., Nyakas, C., and Schoemaker, R.G. (2014). A novel method for evaluating microglial activation using ionized calcium-binding adaptor protein-1 staining: cell body to cell size ratio. Neuroimmunol. Neuroinflamm. *1*, 82–88.

Inoue, D., and Wittbrodt, J. (2011). One for all–a highly efficient and versatile method for fluorescent immunostaining in fish embryos. PLoS ONE *6*, e19713.

Jenkins, S.J., Ruckerl, D., Thomas, G.D., Hewitson, J.P., Duncan, S., Brombacher, F., Maizels, R.M., Hume, D.A., and Allen, J.E. (2013). IL-4 directly signals tissue-resident macrophages to proliferate beyond homeostatic levels controlled by CSF-1. J. Exp. Med. *210*, 2477–2491.

Kim, D., Langmead, B., and Salzberg, S.L. (2015). HISAT: a fast spliced aligner with low memory requirements. Nat. Methods *12*, 357–360.

Konno, T., Tada, M., Tada, M., Koyama, A., Nozaki, H., Harigaya, Y., Nishimiya, J., Matsunaga, A., Yoshikura, N., Ishihara, K., et al. (2014). Haploinsufficiency of CSF-1R and clinicopathologic characterization in patients with HDLS. Neurology *82*, 139–148.

Konno, T., Yoshida, K., Mizuno, T., Kawarai, T., Tada, M., Nozaki, H., Ikeda, S.I., Nishizawa, M., Onodera, O., Wszolek, Z.K., and Ikeuchi, T. (2017). Clinical and genetic characterization of adult-onset leukoencephalopathy with axonal spheroids and pigmented glia associated with CSF1R mutation. Eur. J. Neurol. *24*, 37–45.

Lawrence, M., Huber, W., Pagès, H., Aboyoun, P., Carlson, M., Gentleman, R., Morgan, M.T., and Carey, V.J. (2013). Software for computing and annotating genomic ranges. PLoS Comput. Biol. *9*, e1003118.

Ling, E.A. (1979). Transformation of monocytes into amoeboid microglia in the corpus callosum of postnatal rats, as shown by labelling monocytes by carbon particles. J. Anat. *128*, 847–858.

Luo, J., Elwood, F., Britschgi, M., Villeda, S., Zhang, H., Ding, Z., Zhu, L., Alabsi, H., Getachew, R., Narasimhan, R., et al. (2013). Colony-stimulating factor 1 receptor (CSF1R) signaling in injured neurons facilitates protection and survival. J. Exp. Med. *210*, 157–172.

Matcovitch-Natan, O., Winter, D.R., Giladi, A., Vargas Aguilar, S., Spinrad, A., Sarrazin, S., Ben-Yehuda, H., David, E., Zelada González, F., Perrin, P., et al. (2016). Microglia development follows a stepwise program to regulate brain homeostasis. Science *353*, aad8670.

Merrifield, G.D., Mullin, J., Gallagher, L., Tucker, C., Jansen, M.A., Denvir, M., and Holmes, W.M. (2017). Rapid and recoverable in vivo magnetic resonance imaging of the adult zebrafish at 7T. Magn. Reson. Imaging *37*, 9–15.

Meuwissen, M.E., Schot, R., Buta, S., Oudesluijs, G., Tinschert, S., Speer, S.D., Li, Z., van Unen, L., Heijsman, D., Goldmann, T., et al. (2016). Human USP18 deficiency underlies type 1 interferonopathy leading to severe pseudo-TORCH syndrome. J. Exp. Med. *213*, 1163–1174.

Monies, D., Maddirevula, S., Kurdi, W., Alanazy, M.H., Alkhalidi, H., Al-Owain, M., Sulaiman, R.A., Faqeih, E., Goljan, E., Ibrahim, N., et al. (2017). Autozygosity reveals recessive mutations and novel mechanisms in dominant genes: implications in variant interpretation. Genet. Med. *19*, 1144–1150.

Münzel, E.J., Schaefer, K., Obirei, B., Kremmer, E., Burton, E.A., Kuscha, V., Becker, C.G., Brösamle, C., Williams, A., and Becker, T. (2012). Claudin k is specifically expressed in cells that form myelin during development of the nervous system and regeneration of the optic nerve in adult zebrafish. Glia *60*, 253–270.

Naito, M., Hayashi, S., Yoshida, H., Nishikawa, S., Shultz, L.D., and Takahashi, K. (1991). Abnormal differentiation of tissue macrophage populations in 'osteopetrosis' (op) mice defective in the production of macrophage colony-stimulating factor. Am. J. Pathol. *139*, 657–667.

Nandi, S., Gokhan, S., Dai, X.M., Wei, S., Enikolopov, G., Lin, H., Mehler, M.F., and Stanley, E.R. (2012). The CSF-1 receptor ligands IL-34 and CSF-1 exhibit distinct developmental brain expression patterns and regulate neural progenitor cell maintenance and maturation. Dev. Biol. *367*, 100–113.

Neumann, H., Kotter, M.R., and Franklin, R.J. (2009). Debris clearance by microglia: an essential link between degeneration and regeneration. Brain *132*, 288–295.

Olmos-Alonso, A., Schetters, S.T., Sri, S., Askew, K., Mancuso, R., Vargas-Caballero, M., Holscher, C., Perry, V.H., and Gomez-Nicola, D. (2016). Pharmacological targeting of CSF1R inhibits microglial proliferation and prevents the progression of Alzheimer's-like pathology. Brain *139*, 891–907.

Oosterhof, N., Boddeke, E., and van Ham, T.J. (2015). Immune cell dynamics in the CNS: Learning from the zebrafish. Glia *63*, 719–735.

Oosterhof, N., Holtman, I.R., Kuil, L.E., van der Linde, H.C., Boddeke, E.W., Eggen, B.J., and van Ham, T.J. (2017). Identification of a conserved and acute neurodegeneration-specific microglial transcriptome in the zebrafish. Glia *65*, 138–149.

Oyanagi, K., Kinoshita, M., Suzuki-Kouyama, E., Inoue, T., Nakahara, A., Tokiwai, M., Arai, N., Satoh, J.I., Aoki, N., Jinnai, K., et al. (2017). Adult onset leukoencephalopathy with axonal spheroids and pigmented glia (ALSP) and Nasu-Hakola disease: lesion staging and dynamic changes of axons and microglial subsets. Brain Pathol. *27*, 748–769.

Pagán, A.J., Yang, C.T., Cameron, J., Swaim, L.E., Ellett, F., Lieschke, G.J., and Ramakrishnan, L. (2015). Myeloid Growth Factors Promote Resistance to Mycobacterial Infection by Curtailing Granuloma Necrosis through Macrophage Replenishment. Cell Host Microbe *18*, 15–26.

Paloneva, J., Manninen, T., Christman, G., Hovanes, K., Mandelin, J., Adolfsson, R., Bianchin, M., Bird, T., Miranda, R., Salmaggi, A., et al. (2002). Mutations in two genes encoding different subunits of a receptor signaling complex result in an identical disease phenotype. Am. J. Hum. Genet. *71*, 656–662.

Paolicelli, R.C., Bolasco, G., Pagani, F., Maggi, L., Scianni, M., Panzanelli, P., Giustetto, M., Ferreira, T.A., Guiducci, E., Dumas, L., et al. (2011). Synaptic pruning by microglia is necessary for normal brain development. Science *333*, 1456–1458.

Parichy, D.M., Ransom, D.G., Paw, B., Zon, L.I., and Johnson, S.L. (2000). An orthologue of the kit-related gene fms is required for development of neural crest-derived xanthophores and a subpopulation of adult melanocytes in the zebrafish, Danio rerio. Development *127*, 3031–3044.

Pertea, M., Kim, D., Pertea, G.M., Leek, J.T., and Salzberg, S.L. (2016). Transcript-level expression analysis of RNA-seq experiments with HISAT, StringTie and Ballgown. Nat. Protoc. *11*, 1650–1667.

Prinz, M., and Priller, J. (2014). Microglia and brain macrophages in the molecular age: from origin to neuropsychiatric disease. Nat. Rev. Neurosci. *15*, 300–312.

Rademakers, R., Baker, M., Nicholson, A.M., Rutherford, N.J., Finch, N., Soto-Ortolaza, A., Lash, J., Wider, C., Wojtas, A., DeJesus-Hernandez, M., et al. (2011). Mutations in the colony stimulating factor 1 receptor (CSF1R) gene cause hereditary diffuse leukoencephalopathy with spheroids. Nat. Genet. *44*, 200–205.

Réu, P., Khosravi, A., Bernard, S., Mold, J.E., Salehpour, M., Alkass, K., Perl, S., Tisdale, J., Possnert, G., Druid, H., and Frisén, J. (2017). The Lifespan and Turnover of Microglia in the Human Brain. Cell Rep. *20*, 779–784.

Robinson, M.D., McCarthy, D.J., and Smyth, G.K. (2010). edgeR: a Bioconductor package for differential expression analysis of digital gene expression data. Bioinformatics *26*, 139–140.

Safaiyan, S., Kannaiyan, N., Snaidero, N., Brioschi, S., Biber, K., Yona, S., Edinger, A.L., Jung, S., Rossner, M.J., and Simons, M. (2016). Age-related myelin degradation burdens the clearance function of microglia during aging. Nat. Neurosci. *19*, 995–998.

Sampson, T.R., Debelius, J.W., Thron, T., Janssen, S., Shastri, G.G., Ilhan, Z.E., Challis, C., Schretter, C.E., Rocha, S., Gradinaru, V., et al. (2016). Gut Microbiota Regulate Motor Deficits and Neuroinflammation in a Model of Parkinson's Disease. Cell *167*, 1469–1480.e12.

Sasaki, A., Yokoo, H., Naito, M., Kaizu, C., Shultz, L.D., and Nakazato, Y. (2000). Effects of macrophage-colony-stimulating factor deficiency on the maturation of microglia and brain macrophages and on their expression of scavenger receptor. Neuropathology *20*, 134–142.

Sierra, A., Encinas, J.M., Deudero, J.J., Chancey, J.H., Enikolopov, G., Overstreet-Wadiche, L.S., Tsirka, S.E., and Maletic-Savatic, M. (2010). Microglia shape adult hippocampal neurogenesis through apoptosis-coupled phagocytosis. Cell Stem Cell *7*, 483–495.

Spangenberg, E.E., Lee, R.J., Najafi, A.R., Rice, R.A., Elmore, M.R., Blurton-Jones, M., West, B.L., and Green, K.N. (2016). Eliminating microglia in Alzheimer's mice prevents neuronal loss without modulating amyloid-β pathology. Brain *139*, 1265–1281.

Stevens, B., Allen, N.J., Vazquez, L.E., Howell, G.R., Christopherson, K.S., Nouri, N., Micheva, K.D., Mehalow, A.K., Huberman, A.D., Stafford, B., et al. (2007). The classical complement cascade mediates CNS synapse elimination. Cell *131*, 1164–1178.

Tada, M., Konno, T., Tada, M., Tezuka, T., Miura, T., Mezaki, N., Okazaki, K., Arakawa, M., Itoh, K., Yamamoto, T., et al. (2016). Characteristic microglial features in patients with hereditary diffuse leukoencephalopathy with spheroids. Ann. Neurol. *80*, 554–565.

Teitelbaum, R., Schubert, W., Gunther, L., Kress, Y., Macaluso, F., Pollard, J.W., McMurray, D.N., and Bloom, B.R. (1999). The M cell as a portal of entry to the lung for the bacterial pathogen Mycobacterium tuberculosis. Immunity *10*, 641–650.

Tremblay, M.E., Lowery, R.L., and Majewska, A.K. (2010). Microglial interactions with synapses are modulated by visual experience. PLoS Biol. *8*, e1000527.

Umeda, S., Takahashi, K., Naito, M., Shultz, L.D., and Takagi, K. (1996). Neonatal changes of osteoclasts in osteopetrosis (op/op) mice defective in production of functional macrophage colony-stimulating factor (M-CSF) protein and effects of M-CSF on osteoclast development and differentiation. J. Submicrosc. Cytol. Pathol. *28*, 13–26.

van Ham, T.J., Kokel, D., and Peterson, R.T. (2012). Apoptotic cells are cleared by directional migration and elmo1- dependent macrophage engulfment. Curr. Biol. *22*, 830–836.

van Ham, T.J., Brady, C.A., Kalicharan, R.D., Oosterhof, N., Kuipers, J., Veenstra-Algra, A., Sjollema, K.A., Peterson, R.T., Kampinga, H.H., and Giepmans, B.N. (2014). Intravital correlated microscopy reveals differential macrophage and microglial dynamics during resolution of neuroinflammation. Dis. Model. Mech. *7*, 857–869.

Wang, Y., Szretter, K.J., Vermi, W., Gilfillan, S., Rossini, C., Cella, M., Barrow, A.D., Diamond, M.S., and Colonna, M. (2012). IL-34 is a tissue-restricted ligand of CSF1R required for the development of Langerhans cells and microglia. Nat. Immunol. *13*, 753–760.

Wegiel, J., Wiśniewski, H.M., Dziewiatkowski, J., Tarnawski, M., Kozielski, R., Trenkner, E., and Wiktor-Jedrzejczak, W. (1998). Reduced number and altered morphology of microglial cells in colony stimulating factor-1-deficient osteopetrotic op/op mice. Brain Res. *804*, 135–139.

Wider, C., Van Gerpen, J.A., DeArmond, S., Shuster, E.A., Dickson, D.W., and Wszolek, Z.K. (2009). Leukoencephalopathy with spheroids (HDLS) and pigmentary leukodystrophy (POLD): a single entity? Neurology *72*, 1953–1959.

Wlodarczyk, A., Holtman, I.R., Krueger, M., Yogev, N., Bruttger, J., Khorooshi, R., Benmamar-Badel, A., de Boer-Bergsma, J.J., Martin, N.A., Karram, K., et al. (2017). A novel microglial subset plays a key role in myelinogenesis in developing brain. EMBO J. *36*, 3292–3308.

Wynn, T.A., Chawla, A., and Pollard, J.W. (2013). Macrophage biology in development, homeostasis and disease. Nature *496*, 445–455.

Young, M.D., Wakefield, M.J., Smyth, G.K., and Oshlack, A. (2010). Gene ontology analysis for RNA-seq: accounting for selection bias. Genome Biol. *11*, R14.

Zhang, Y., Chen, K., Sloan, S.A., Bennett, M.L., Scholze, A.R., O'Keeffe, S., Phatnani, H.P., Guarnieri, P., Caneda, C., Ruderisch, N., et al. (2014). An RNA-sequencing transcriptome and splicing database of glia, neurons, and vascular cells of the cerebral cortex. J. Neurosci. *34*, 11929–11947.

Zhang, J., Lachance, V., Schaffner, A., Li, X., Fedick, A., Kaye, L.E., Liao, J., Rosenfeld, J., Yachelevich, N., Chu, M.L., et al. (2016). A Founder Mutation in VPS11 Causes an Autosomal Recessive Leukoencephalopathy Linked to Autophagic Defects. PLoS Genet. *12*, e1005848.

STAR★METHODS

KEY RESOURCES TABLE

REAGENT or RESOURCE	SOURCE	IDENTIFIER
Antibodies		
Rabbit anti-zebrafish L-plastin	Yi Feng, University of Edinburgh	N/A
Rabbit polyclonal anti-Sox10	Genetex	Cat#GTX128374
Mouse anti-Pcna	Dako	Cat#M0879; RRID: AB_2160651
DyLight alexa 488 anti-rabbit	ThermoFisher Scientific	Cat#711-545-152; RRID: AB_2313584
DyLight alexa 488 anti-mouse	ThermoFisher Scientific	Cat#715-545-150; RRID: AB_2340846
DyLight alexa 647 anti-rabbit	ThermoFisher Scientific	Cat#711-605-152; RRID: AB_2492288
DyLight alexa 647 anti-mouse	ThermoFisher Scientific	Cat#715-605-150; RRID: AB_2340862
Alexa 594 goat anti-rat	Invitrogen	Cat#A11007; RRID: AB_141374
Rat anti-Claudin K (Thomas Becker, University of Edinburgh)	Münzel et al., 2012	PMID:22020875
Rabbit anti-human IBA1	Wako Chemicals	Cat#019-19741; RRID: AB_839504
Mouse anti-human CD68 (clone KP-1)	Abcam	Cat#ab955; RRID: AB_307338
Anti-rabbit HRP	Dako	Cat#P0217; RRID: AB_2728719
biotinylated goat anti-rabbit antibodies	Vector Laboratories	Cat#BA-1000; RRID: AB_2313606
Goat-serum	Dako	Cat#X090710
Biological Samples		
Human paraffin embedded cortical brain tissues	the Netherlands Brain Bank	https://www.brainbank.nl/
(See for details Table S1)		
Chemicals, Peptides, and Recombinant Proteins		
1-phenyl 2-thiourea (PTU)	Sigma Aldrich	Cat#P7629
low melting point (LMP) agarose	ThermoFisher	Cat#16520050
3,3′-diaminobenzidine (DAB)	Sigma-Aldrich	Cat#D8001
Metronidazole	Sigma-Aldrich	Cat#M3761
Entellan	Merck	Cat#1079610100
Protifar	Nutricia	N/A
Mowiol	Sigma	Cat#81381
Paired end adapters with dual index	Illumina	Cat#PE-121-1003
Bovine serum albumin	Sigma-Aldrich	Cat#A2058
Luxol Fast Blue	Fisher Scientific	Cat#AC212170250
Uranyl acetate	Merck	Cat#8473
Glutaraldehyde	Polysciences	Cat#1909
Sodium cacodylate	Sigma	Cat#C0250
Osmiumtetroxide	Electron Microscopy Sciences	Cat#19114
Potassiumferrocyanide ($K_4[Fe(CN)]_6$)	Merck	Cat#4984
EPON resin		
2-dodecenylsuccinicacid anhydride	Serva	Cat#20755
methylnadic anhydride	Serva	Cat#29452
glycid ether 100	Serva	Cat#21045
DMP-30	Polysciences	Cat#553
Critical Commercial Assays		
TruSeq SR Rapid Cluster kit v2 (cBot)	Illumina	Cat#GD-300-2001

(*Continued on next page*)

Continued

REAGENT or RESOURCE	SOURCE	IDENTIFIER
Deposited Data		
Zebrafish control and *csf1r* mutant microglia RNA-sequencing data	This study	https://www.ncbi.nlm.nih.gov/geo/query/acc.cgi?acc=GSE116217
Zebrafish control and *csf1r* mutant brain RNA-sequencing data	This study	https://www.ncbi.nlm.nih.gov/geo/query/acc.cgi?acc=GSE116217
Experimental Models: Organisms/Strains		
csf1rb$^{re01/re01}$ mutant zebrafish generated by TALEN carrying a 4 bp deletion in exon 3	This study	N/A
Tg(*mpeg1*:*EGFP*) zebrafish	Ellett et al., 2011	ZDB-TGCONSTRCT-120117-1
csf1ra$^{j4e1/j4e1}$ mutant zebrafish	Parichy et al., 2000	N/A
Tg(UAS-E1b:NTR-mCherry) zebrafish	Davison et al., 2007	ZDB-FISH-150901-2592
Et(shhb:KalTA4,UAS-E1b:mCherry)zf279, Mu4465_13		ZDB-ALT-120221-7
Oligonucleotides		
csf1rb TALEN vectors	This paper	N/A
csf1rb primer genotyping forward: CTTGCTGAC AAATCCAGCAG	This paper	N/A
csf1rb primer genotyping reverse: AAACTAAAT GCGGCCATACG	This paper	N/A
csf1ra forward: CAAAGCACTTCATGGGACCT	This paper	N/A
csf1ra reverse: CATTACCACACCGACACAGC	This paper	N/A
csf1ra on WT allele: AAGAGGACAACATCACACGAG	This paper	N/A
csf1ra on mutant allele: AAGAGGACAA CATCACACGAA	This paper	N/A
Recombinant DNA		
Golden Gate TALEN and TALEffector Kit 2.1 (Addgene)	Cermak et al., 2011	Cat#1000000024
Software and Algorithms		
Bioconductor package edgeR	Robinson et al., 2010	https://bioconductor.org/packages/release/bioc/html/edgeR.html
Bioconductor package Genomic Ranges	Lawrence et al., 2013	https://bioconductor.org/packages/release/bioc/html/GenomicRanges.html
HiSat2 aligner (version 2.0.4)	Pertea et al., 2016	https://ccb.jhu.edu/software/hisat2/index.shtml
Goseq	Young et al., 2010	https://bioconductor.org/packages/release/bioc/html/goseq.html
biomaRt	Durinck et al., 2009	https://bioconductor.org/packages/release/bioc/html/biomaRt.html

CONTACT FOR REAGENT AND RESOURCE SHARING

Further information and requests for resources and reagents should be directed to and will be fulfilled by the Lead Contact, Tjakko van Ham (t.vanham@erasmusmc.nl).

EXPERIMENTAL MODEL AND SUBJECT DETAILS

Animal models

All zebrafish were maintained under standard conditions. Adult animals were kept in groups on a 14 hr light and 10 hr dark cycle. They were fed brine shrimp twice a day. Embryos were kept at 28°C in 10 mM HEPES-buffered E3 embryo medium. In larvae analyzed between 3-5 dpf sex-determination has not yet occurred. For microglia RNA-sequencing experiments groups of 3 animals were used, containing at least 1 male and 1 female. For whole brain RNA-sequencing groups of 3 animals, 1 male and 2 females, were used. The following existing transgenic or mutant zebrafish lines were used: Wild-type AB, Tg(*mpeg1*:*EGFP*) fish expressing GFP under the control of the *mpeg1* promotor (Ellett et al., 2011), Tg(shhb:KalTA4,UAS-E1b:mCherry, *UAS-E1b:NTR-mCherry*,

mpeg1:*EGFP*) with neuronal specific *nsfB* expression encoding nitroreductase (NTR)(Davison et al., 2007; van Ham et al., 2014), *csf1ra*$^{j4e1/j4e1}$ with a V614M substitution in the first kinase domain (Parichy et al., 2000). *Csf1ra* mutants were also crossed in with the transgenic lines specified above. The *csf1rb* deletion mutant was created by TALEN-mediated genome editing (Cermak et al., 2011). The TALEN arms targeted exon 3 (Figure S1) of the *csf1rb* gene, resulting in a 4 bp deletion and premature stop codon. These zebrafish deficient in *csf1rb, csf1rb*$^{re01/re01}$, lose an *MspI* restriction site which was used for genotyping. Animal experiments were approved by the Animal Experimentation Committee at Erasmus MC, Rotterdam.

Human post mortem brain tissue

Human brain tissue samples were obtained from the Netherlands Brain Bank (https://www.brainbank.nl/). All patients and controls, or their next of kin, had given informed consent for autopsy and the use of brain tissue for research purposes. Relevant clinical information was retrieved from the medical records and is summarized in Table S1. We obtained paraffin-embedded post mortem tissue blocks of cingulate gyrus, frontal cortex, and occipital lobe from 2 ALSP patients and 2 age-matched controls without neurological disease.

METHOD DETAILS

Vital dye labeling

Neutral red labeling was performed as described previously (Herbomel et al., 2001). For all experiments in larvae, embryos were kept in E3 medium containing 0.003% 1-phenyl 2-thiourea (PTU) (Sigma-Aldrich) from 22 hpf onward. To assess microglia numbers, 5 or 6 dpf larvae were treated with 2.5 μg/ml neutral red in E3+PTU medium at 28°C for two hr. After two hr, larvae were incubated in E3+PTU for at least 30 min before imaging. For imaging, larvae were anesthetized with 0.016% MS-222 (Sigma-Aldrich) and embedded in 1.8% low melting point (LMP) agarose (VWR BDH Prolabo) with the dorsal side facing upward. Neutral red images were acquired by using a Leica M165FC stereo microscope.

Conditional neuronal cell death

For neuronal ablation, neuro-NTR transgenic zebrafish were used as described previously (Davison et al., 2007; van Ham et al., 2014).

Larvae were treated with 2 mM metronidazole (MTZ) dissolved in DMSO at 28°C for 16 hr. MTZ was washed away with E3+PTU medium. Larvae were euthanized and fixed at different times after the start of treatment, at 1 day post treatment (20 h) and 2 days post treatment (48 h).

Immunofluorescence staining

Whole mount larvae This was usually done as described previously (Inoue and Wittbrodt, 2011). Larvae were fixed in 4% PFA at 4°C overnight, dehydrated to 100% MeOH, and kept at −20°C for at least two days. They were then rehydrated to PBSTw (PBS + 0.1% Tween). Antigens were retrieved by incubating the larvae in 150 mM Tris-HCl pH = 9.0 for 5 min, followed by incubation at 70°C for 15 min. Afterward, larvae were washed with PBSTw (2x 10 min) and dH_2O (2x 5 min) and incubated in acetone at −20°C for 20 min. This was followed by several washing steps in PBSTw (6x 5 min); dH2O (2x 5 min); and PBSTw (2x 5 min). The larvae were then incubated in blocking buffer (10% goat serum, 1% Triton X-100, 1% BSA in PBSTw) at 4°C for 3h. Primary-antibody labeling (1st antibody in 1% goat serum, 0.8% Triton X-100, 1% BSA in PBSTw) was done at 4°C for three days. Larvae were washed in PBS-TS (10% goat serum, 1% Triton X-100 in PBS) (3x 1h); PBST (1% Triton X-100 in PBS) (2x 10 min); and PBS-TS (2x 1 h). The larvae were then incubated with the secondary antibody and Hoechst at 4°C for 2.5 days. Before imaging, the larvae were washed with PBS-TS (3x 1 h); and PBSTw (2x 1 h). Primary antibodies: PCNA (1:250, Dako); and L-plastin (1:500; gift from Yi Feng, University of Edinburgh). Secondary antibodies: DyLight alexa 488 (1:500); and DyLight alexa 647 (1:500). Hoechst was used for nuclear staining. Images were taken with a Leica SP5 confocal microscope using a 20x water dipping lens (NA = 1.0). Total microglia numbers were quantified for the entire brain. The microglia response to neuronal death was quantified in the larval forebrain.

Adult brain sections

Immunostaining on adult brain slices was performed largely as described previously (Oosterhof et al., 2017). Fish were euthanized in ice water, after which the skull (containing the brain) was fixed in 4% PFA at 4°C overnight. Subsequently, the brains were carefully removed and dehydrated with a 25%, 50%, 75%, 100% MeOH series and kept at −20°C for at least 12 hr. After rehydration, brains were embedded in 4% w/v low melting point agarose in PBS and cut into 80 μm horizontal sections using a Microm HM 650V vibratome (ThermoFisher Scientific). Immunostainings on free-floating sections were performed as described. The sections were incubated in blocking buffer (10% goat serum, 0.5% Triton X-100 in PBS) at room temperature for 75 min, followed by incubation with the primary antibody in blocking buffer at 4°C overnight. The sections were thoroughly washed with PBST (0.5% Triton X-100) before incubation with the secondary antibody and Hoechst at 4°C overnight. The brain slices were then washed with PBST (5 × 30-60 min) and mounted on microscope slides using vectashield mounting medium H1000 (Vector Laboratories). Primary antibodies: L-plastin (1:1000; gift from Yi Feng, University of Edinburgh); ClaudinK (1:1000; gift from Thomas and Catherina Becker, Edinburgh); and Sox10 (1:500, Genetex). Secondary antibodies used were DyLight alexa 488 and DyLight alexa 647 (1:500, ThermoFisher Scientific, Waltham, US), and alexa 594 (1:250, Invitrogen, Waltham, US). Imaging was done with a Zeiss LSM700 confocal microscope using a 20x lens (NA = 0.75).

Immunohistochemistry zebrafish paraffin sections

4.5 month old zebrafish were euthanized in ice water and fixated in 4% PFA at 4°C over the weekend. Thereafter fish were washed in PBS before transferring them to 20% EDTA at room temperature for weeks for the bone to decalcify. Fish were embedded in paraffin and 10μm sections were cut and dried overnight at 37°C. Sections were deparaffinized and rehydrated to distilled water. Antigen retrieval was performed by heating in 0.01M sodium citrate pH = 6 for 13 min. After cooling slices were rinsed with PBS before blocking endogenous peroxidase activity by 30 min incubation in 0.6% H_2O_2, 1.5% sodium azide in PBS at room temperature. Slides were rinsed in PBS+ (0.5% protifar, 0.15% glycine) before L-plastin antibody incubation (1:1000) overnight at 4°C in PBS+. Slides were rinsed with PBS+ before incubation with conjugated secondary antibody (anti-rabbit-HRP 1:100) for 60 min at room temperature. After washing in PBS+ and PBS slides were incubated in DAB-substrate (DAKO liquid DAB substrate-chromogen system). After washing with distilled water a counterstaining with hematoxylin was performed for 5 min. After washing in distilled water slices were dehydrated and mounted with Entellan (Merck).

Paraffin sections human brain

Tissue sections were characterized for the presence of microglia by staining for IBA1, HLA-DR and CD68 as previously described (Hovens et al., 2014). Paraffin sections seven μm in thickness were collected on Superfrost Plus glass slides (VWR international, Leuven, Belgium) and dried at 37°C overnight. Tissue sections were deparaffinized and rehydrated to distilled water. Endogenous peroxidase was quenched in 0.3% H_2O_2 (Merck, Darmstadt, Germany) in phosphate-buffered saline (PBS), and antigen was retrieved by heating the slides in citrate buffer (10 mM; pH 6.0). The sections were then incubated with normal horse serum blocking buffer (TBS supplemented with 2% horse serum, 1% bovine serum albumin (Sigma-Aldrich, St. Louis, USA); 0.1% Triton X-100 and 0.05% Tween (Merck)) for 30 min at RT. Thereafter, sections were incubated with rabbit anti-human IBA1 antibodies (1:1000 TBS-BSA 1%; WAKO Chemicals, Richmond, USA) overnight at 4°C. After rinsing, the sections were incubated with biotinylated goat anti-rabbit antibodies (1:400 in TBS-BSA 1%; Vector Laboratories, Burlingame, USA) for 1 h at RT; this was followed by incubation with the avidin-biotin complex (1:800 in TBS; Vector Laboratories) for 45′ at RT, The sections were then developed with 3,3′-diaminobenzidine (DAB; 0.05 mg/ml, Sigma-Aldrich). After washing in distilled water, slides were dehydrated and embedded in Entallan (Merck). In between all steps, sections were extensively rinsed in TBS. Whole slides were digitalized using a NanoZoomer digital slide scanner (Hamamatsu) and the slides were analyzed using Hamamatsu software NDPview2. The numbers of $IBA1^+$ microglia were quantified in 5 areas of 1.5 mm^2 per brain region per patient.

For the CD68/IBA1 immunofluorescent double-staining, tissue sections were deparaffinized and rehydrated to distilled water. Antigen retrieval was performed by heating the slides in citrate buffer (10 mM; pH 6.0). Sections were then rinsed in blocking buffer (PBS, 0.5% protifar (Nutricia), 0.15% glycine (Sigma-Aldrich, St. Louis, USA), 0.4% Triton X-100) for 2 times 2 min at RT. Thereafter, sections were incubated with blocking buffer containing rabbit anti-human IBA1 (1:500, WAKO Chemicals, Richmond, USA) and mouse anti-human CD68 (1:50, clone KP-1) antibodies overnight at 4°C. After rinsing with blocking buffer, sections were incubated with secondary anti-rabbit Alexa 488 (1:200, ThermoFisher Scientific, Waltham, US) and anti-mouse Cy3 antibodies (1:200) for 1h at RT. Autofluorescence was blocked by incubating slides in Sudan Black solution for 5 min at RT. After washing the slides were embedded in Mowiol containing DAPI.

Luxol fast blue staining

Paraffin sections seven μm in thickness were collected on glass slides (Superfrost Plus, VWR international, Leuven, Belgium) and dried at 37°C. Sections were deparaffinized and hydrated to 95% ethanol and incubated in Luxol fast blue solution (0.1% w/v luxol fast blue, Sigma-Aldrich, in 95% ethanol) overnight at 55°C. The sections were then quickly rinsed in 95% ethanol and incubated in lithium carbonate solution (0.05% w/v, Sigma-Aldrich, in distilled H_2O) for 30 s. Next, the samples were rinsed in 70% ethanol and subsequently in ddH2O. The sections were dehydrated to 100% ethanol and mounted with Entallan (Merck). Whole slides were digitalized using a NanoZoomer digital slide scanner (Hamamatsu), and the slides were analyzed using Hamamatsu software NDPview2.

RNA sequencing

Whole brain

For whole brain transcriptomic analysis brains were dissected as described previously (Oosterhof et al., 2017) and snap frozen in liquid nitrogen. Zebrafish between 6-12 mpf were used. Zebrafish were euthanized in ice water and heads were severed behind the gills, and the lower jaw, gills, and eyes were removed. The brains were taken out of the skull and cut using scalpels. Brains were homogenized followed by total RNA isolation using Trizol. Total RNA quality for triplicates of WT brain, $csf1ra^{-/-}$ brain, $csf1ra^{-/-};b^{+/-}$ brain and $csf1r^{DM}$ brain was assessed on an Agilent Technologies 2100 Bioanalyzer using a RNA nano assay. All samples had RIN value greater than 9.10. Triplicate RNA-seq libraries were prepared according to the Illumina TruSeq stranded mRNA protocol (https://www.illumina.com). Briefly, 200 ng of total RNA was purified using poly-T oligo-attached magnetic beads to end up with poly-A containing mRNA. The poly-A tailed mRNA was fragmented and cDNA was synthesized using SuperScript II and random primers in the presence of Actinomycin D. cDNA fragments were end repaired, purified with AMPure XP beads, A-tailed using Klenow exo-enzyme in the presence of dATP. Paired end adapters with dual index (Illumina) were ligated to the A-tailed cDNA fragments and

purified using AMPure XP beads. The resulting adaptor-modified cDNA fragments were enriched by PCR using Phusion polymerase as followed: 30 s at 98°C, 15 cycles of (10 s at 98°C, 30 s at 60°C, 30 s at 72°C), 5 min at 72°C. PCR products were purified using AMPure XP beads and eluted in 30 μl of resuspension buffer. One microliter was loaded on an Agilent Technologies 2100 Bioanalyzer using a DNA 1000 assay to determine the library concentration and for quality check.

Bridge amplification, sequencing by synthesis and data analysis

Cluster generation was performed according to the Illumina TruSeq SR Rapid Cluster kit v2 (cBot) Reagents Preparation Guide (https://www.illumina.com/). Briefly, 12 RNA-seq libraries were pooled together to get a stock of 10 nM. One microliter of the 10 nM stock was denaturated with NaOH, diluted to 6 pM and hybridized onto the flowcell. The hybridized products were sequentially amplified, linearized, and end-blocked according to the Illumina Single Read Multiplex Sequencing user guide. After hybridization of the sequencing primer, sequencing-by-synthesis was performed using the HiSeq 2500 with a single read 50-cycle protocol followed by dual index sequencing. Reads were aligned against the GRCz10 genome using HiSat2 (version 2.0.4) (Kim et al., 2015). Counts were generated for each gene from the Ensembl (version 85) transcriptome analysis of GRCz10, using htseq-count (version 0.6.0) (Anders et al., 2015).

Microglia

Tg(*mpeg1*:*EGFP*) zebrafish were euthanized in ice water. The heads were severed behind the gills, and the lower jaw, gills, and eyes were removed. The brains (4-5 per sample) were taken out of the skull and cut using scalpels. This was followed by dissociation in 0.25% trypsin and 0.1% EDTA in PBS for 2 hr at 4°C, while resuspending regularly. Upon complete dissociation of the brain, trypsin was inactivated by adding 1/6 volume of a stop solution (6 mM $CaCl_2$ in PBS). The cells were collected in a 22% Percoll solution after being run through a 70 μm cell strainer, and ice-cold PBS was placed on top of the cell suspension and centrifuged at 1000 x g at 4°C for 45 min. The remaining cell pellet was resuspended in suspension solution (high-glucose DMEM without phenol red, 0.8 mM $CaCl_2$). The cell suspension was transferred to FACS tubes with 35 μm cell strainer caps and FAC-sorted using a FACSaria III cell sorter (BD biosciences, New Jersey, USA). Dapi was added to exclude dead cells.

RNaseq library synthesis and bioinformatics analysis

Microglia were lysed and processed for RNA-seq largely as described (Oosterhof et al., 2017). FAC-sorted microglia were collected and lysed in RNase-free water containing 0.2% v/v Triton X-100 and RNase inhibitor. PolyA+ RNA was reverse transcribed using an oligo(dT) primer. Template switching by reverse transcriptase was achieved by using an LNA containing TSO oligo. The reverse-transcribed cDNA was pre-amplified with primers for 18 cycles followed by clean-up. Tagmentation was performed on 500 pg of the pre-amplified cDNA with Tn5 followed by gap repair. The tagmented library was extended with Illumina adaptor sequences by PCR for 14 cycles and then purified. The resulting sequencing library was measured on Bioanalyzer and equimolar samples were loaded onto a flowcell and sequenced according to the Illumina TruSeq v3 protocol on the HiSeq2500 with a single-read 50 bp and dual 9 bp indices. The sequencing reads were mapped against the GRCz10 zebrafish genome using the HiSat2 aligner (Pertea et al., 2016). To quantify the aligned and filtered data, the Bioconductor package Genomic Ranges was used (Lawrence et al., 2013). Differential gene expression analysis was performed using the Bioconductor package edgeR (Robinson et al., 2010). To assess the differentiation status of *csf1r* mutant microglia, the differential gene expression list was compared with previously published microglia expression profiles obtained in zebrafish and mice (Bennett et al., 2016; Matcovitch-Natan et al., 2016; Oosterhof et al., 2017). We used the Bioconductor tool Biomart to find high-confidence zebrafish orthologs for the genes from studies performed in mice (Durinck et al., 2009). For gene ontology analysis the Bioconductor package goseq was used (Young et al., 2010).

Electron microscopy

Electron microscopy was performed largely as described previously (van Ham et al., 2014). 4 to 5-month-old zebrafish were euthanized in ice water. The brains were carefully removed and incubated in Zamboni's fixative (4% PFA, 2% glutaraldehyde, 0.2% picric acid, 0.1M cacodylate, pH = 7.4) at 4°C overnight. Brains were washed in cacodylate (3x5 min) and postfixed in a solution containing 1% osmium tetroxide (OsO_4) and 1.5% potassium ferrocyanide ($K_4Fe(CN)_6$) on ice for 2 hr. The brains were then washed in milliQ water (3x5 min) and dehydrated in series of 30%, 50%, 70% ethanol (10 min each), followed by 3 × 20 min incubation in absolute ethanol. Brains were rinsed in acetone, followed by incubation in a 1:1 EPON:acetone solution overnight. Next, the brains were incubated in pure EPON for 1 hr. New EPON was added followed by incubation in EPON for 2 hr. Samples were put at 200 mbar vacuum for 30 min at 37°C. Polymerization took place at 58°C for 3 days. Ultra-thin sections were subsequently cut, collected on formvar-coated single-slot grids, and stained with a 1% aqueous uranyl acetate solution for 20 min and subsequently for 1 min with lead citrate. Photographs were obtained using a JEOL 1010 electron microscope. For each myelinated axon present the axonal diameter (defined by the inner limit of the myelin sheath) and total fiber diameter (defined by the outer limit of the myelin sheath) were measured using FIJI and the g-ratio was calculated by dividing the axonal diameter by the total fiber diameter (Camargo et al., 2017). Each group consisted of two to three zebrafish, and contained at least 240 myelinated fibers per genotype.

QUANTIFICATION AND STATISTICAL ANALYSIS

GraphPad Prism 6 software (La Jolla, CA) was used for statistical tests including one-way ANOVA with Bonferroni multiple testing correction and data are presented as mean ± SD as indicated. For Figures 1 and 5, quantification was done blinded as larval progeny

were genotyped after quantification, and sample sizes depend on the –Mendelian- distribution of genotypes. For analysis of adult brains sample sizes (n = 3-4) are similar to those in previous publications (Oosterhof et al., 2017). A *p* value smaller than 0.05 was considered as significant.

DATA AND SOFTWARE AVAILABILITY

The accession number for the gene level RNA-sequencing data from freshly isolated microglia and brain from control and *csf1r* mutant zebrafish reported in this paper is GEO: GSE116217.